ACS Biomaterials SCIENCE & ENGINEERING

pubs.acs.org/journal/abseba Article

Pharmacokinetic and Pharmacodynamic Evaluation of Resveratrol Loaded Cationic Liposomes for Targeting Hepatocellular Carcinoma

Satveer Jagwani,*,⊥ Sunil Jalalpure,* Dinesh Dhamecha,⊥ Kiran Jadhav, and Raghvendra Bohara

Cite This: https://dx.doi.org/10.1021/acsbiomaterials.0c00429 Read Online

ACCESS | Metrics & More | Article Recommendations | Supporting Information

ABSTRACT: Hepatocellular carcinoma (HCC) is one of the leading causes of cancer-related death worldwide. The destructive nature of the disease makes it difficult for clinicians to manage the condition. Hence, there is an urgent need to find new alternatives for HCC, as the role of conventional cytotoxic drugs has reached a plateau to control HCC associated mortality. Antioxidant compounds of plant origin with potential anti-tumor effect have been recognized as alternate modes in cancer treatment and chemoprevention. Resveratrol (RS) is a model natural nonflavonoid drug known for its anti-cancer activity. However, its clinical application is limited due to its poor bioavailability. The current research work aims to formulate, optimize, and characterize RS loaded cationic liposomes (RLs) for specific delivery in HCC. The optimized liposomes formulation (RL5) was spherical with a vesicle size (VS) of 145.78 ± 9.9 nm, ζ potential (ZP) of 38.03 ± 9.12 mV, and encapsulation efficiency (EE) of 78.14 ± 8.04%. *In vitro* cytotoxicity studies in HepG2 cells demonstrated an improved anti-cancer activity of RL5 in comparison with free RS. These outcomes were supported by a cell uptake study in HepG2 cells, in which RL5 exhibited a higher uptake than free RS. Furthermore, confocal images of HepG2 cells after 3 and 5 h of incubation showed higher internalization of coumarin 6 (C6) loaded liposomes (CL) as compared to those of the free C6. Pharmacokinetic and pharmacodynamic (prophylactic and therapeutic treatment modalities) studies were performed in *N*-nitrosodiethylamine (NDEA-carcinogen) induced HCC in rats. Pharmacokinetic evaluation of RL5 demonstrated increased localization of RS in cancerous liver tissues by 3.2- and 2.2-fold increase in AUC and Cmax, respectively, when compared to those of the free RS group. A pharmacodynamic investigation revealed a significant reduction in hepatocyte nodules in RL5 treated animals when compared to those of free RS. Further, on treatment with RL5, HCC-bearing rats showed a significant decrease in the liver marker enzymes (alanine transaminase, alkaline phosphatase, aspartate transaminase, total bilirubin levels, γ-glutamyl transpeptidase, and α-fetoprotein), in comparison with that of the disease control group. Our findings were supported by histopathological analysis, and we were first to demonstrate that NDEA induced detrimental effect on rat livers was successfully reversed with the treatment of RL5 formulation. These results implied that delivery of RS loaded cationic liposomes substantially controlled the severity of HCC and that they can be considered as a promising nanocarrier in the management of HCC.

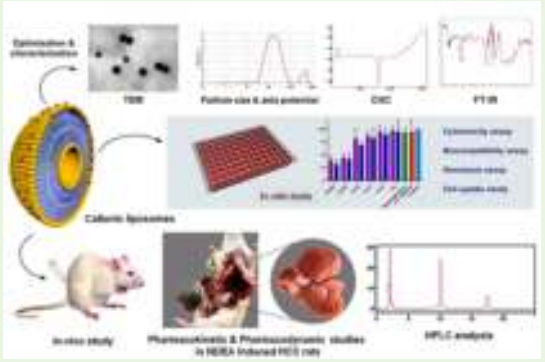

KEYWORDS: *Resveratrol, cationic liposomes, biocompatibility, hepatocellular carcinoma, pharmacokinetics, pharmacodynamics*

1. INTRODUCTION

Noncommunicable diseases (NCD) are one of the significant causes of mortality in the 21st century, in which cancer stands on top of the list, reducing the life expectancy to significant levels worldwide. As per the GLOBOCAN 2018 report, cancer accounts for 20.3, 14.4, 57.3, and 7.3% mortality rates in Europe, USA, Asia, and Africa, respectively.[1] Hepatocellular carcinoma (HCC) is the fourth-leading cause of cancer-related deaths, which has led to a total of 841 080 new cases and 781 631 deaths in the year 2018 worldwide. Hence, there is an alarming need to improve novel drug delivery strategies in HCC.[1]

Currently, HCC is treated with invasive surgical and chemotherapeutical approaches, which often lead to serious side effects such as hand−foot syndrome and gastrointestinal, skin, and endocrine disorders.[2] Furthermore, these conventional approaches have not been successful in reducing the overall mortality rate. Currently, sorafenib (Nexavar) is the only USFDA approved drug for systemic administration in the management of advanced HCC. Active efforts have been made in the past to develop similar therapies, with some of the ongoing phases III trials focused on shedding light on cancer therapy with better outcomes and minimal/no side effects.[3]

Received: March 26, 2020
Accepted: July 27, 2020
Published: July 27, 2020

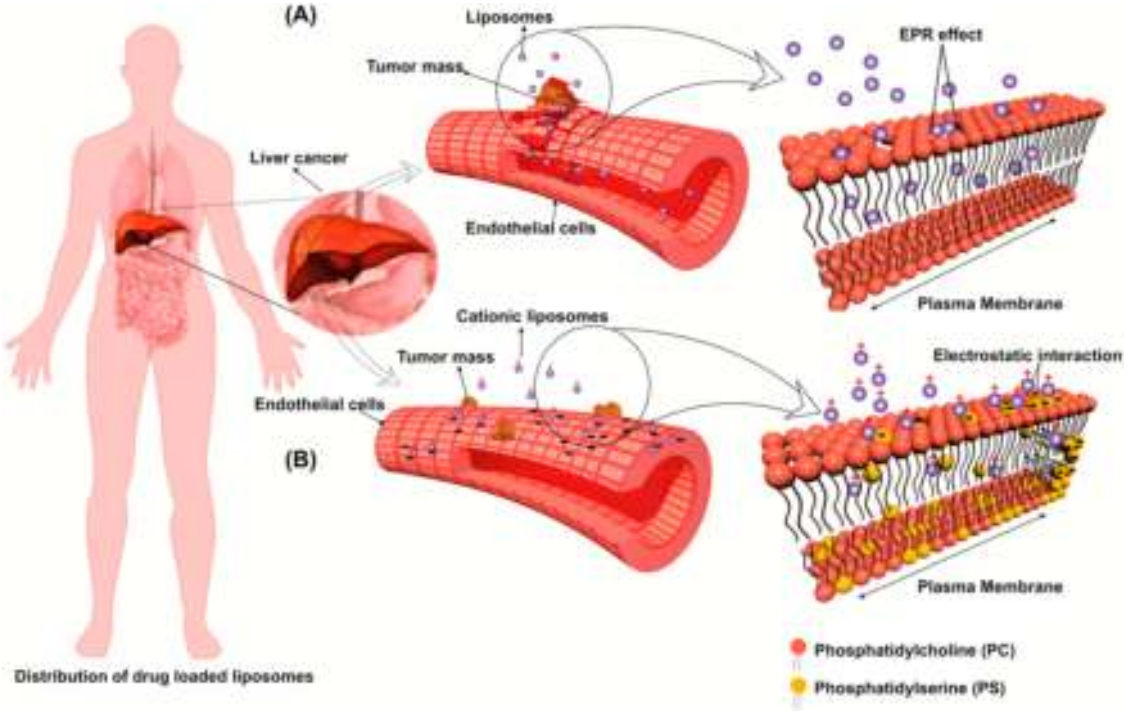

Figure 1. Depicting the mechanism of accumulation/targeting of cationic liposomes in the liver cancer. (A) Enhanced permeability and retention effect (EPR) in which the RLs with appropriate sizes (<200 nm) extravasate through large fenestrations between the tumor blood capillary endothelium (leaky endothelium) and enters the interstitial space. The gaps between the cancer endothelial cells are in the range 100−780 nm as opposed to those of a healthy endothelium, which are 5−10 nm. (B) Targeting of RLs based on the electrostatic interaction between anionic liver cells and cationic liposomes. In the plasma membrane of normal healthy cells, lipids are asymmetrically distributed across the inner and outer leaflets, with phosphatidylserine (PS) being the most abundant anionic phospholipid located predominantly on the inner leaflet. Due to the activation of the scramblase enzyme or oxidative stress in the tumor microenvironment, the symmetry of plasma membrane is lost, resulting in the exposure of PS on the surface, which is a unique feature of cancerous cells. RS loaded cationic liposomes are an easy way to target the anionic moiety of plasma membrane due to electrostatic interaction between them.

In the human body, the liver is the main detoxifying organ responsible for eliminating the metabolic byproducts/toxins to achieve homeostasis. However, the liver is susceptible to the accumulation of reactive oxidative species (ROS) due to imbalance between pro-oxidant and antioxidant compounds. Scientific literature suggests that there is a significant correlation between the increased levels of oxidative stress generated by these reactive oxygen species (ROS) and the severity of chronic liver diseases. It should be noted that HCC occurs in the background of chronic liver disease, making it often difficult to diagnosis at an initial stage.[4]

Antioxidant compounds of plant origin with potential anti-tumor effects have been recognized as alternate modes in cancer chemoprevention. Different phytochemicals, including nutrients and dietary agents, have been found to be effective against numerous types of cancers. Among the various available groups of natural products and plant metabolites, resveratrol (RS), a phytoalexin (plant antibiotic and anti-oxidant) found in peanuts, grapes, pines, berries, and various herbs such as *Polygonum cuspidatum* and *Vitis vinifera* L., plays an essential role as an antioxidant,[5] anti-tumor,[6] anti-aging,[7] anti-diabetic,[8] anti-inflammatory,[9] cardioprotective,[10] and anti-obesity.[11]

Looking toward the potential benefits of RS, its use in prophylaxis and therapeutics would be of great importance in the treatment of HCC. However, the use of free RS in the treatment of human cancer possesses certain limitations owing to the rapid metabolism and swift elimination from systemic circulation, resulting in low bioavailability (<1% oral viability) and low biological half-life (30−45 min).[12,13] Among several nanoparticles (poly-lactic-*co*-glycolic acid,[14,15] gold,[16,17] silver,[18] liposomes,[19] etc.) approaches, liposomes are the most successfully nanoscale formulations used to deliver therapeutic drugs and imaging agents. Encapsulating drugs in lipids offers structural properties similar to the natural cellular biomembrane, which provides several advantages including biocompatibility, higher stability, sustained release of the drug, biodegradability, safety, and industrial scalability.[20−22] Though there are reports for the use of RS loaded liposomes (RLs) in cancers such as cervical cancer,[23] skin cancer,[24−26] glioblastoma,[27] breast cancer,[28] and prostate cancer,[29] the efficacy of RL was never assessed for its use in the treatment of HCC. In HCC, the physiological changes in the surface properties of liver tissue generate large fenestration in the endothelium and anionic charge due to exposed phosphatidylserine (PS). These anionic moieties are exposed to the outer surface, which makes it an easy target to attract cationic liposomes for active targeting of liposomes. A schematic diagram depicting the probable targeting mechanism is shown in Figure 1.[30,31]

With this background, the present study aimed to encapsulate RS in a unique blend of a lipid and cationic charge generator for the formulation of cationic liposomes for selective delivery in HCC. The performance of optimized RL5 was evaluated with *in vitro* cytotoxicity assay, cellular uptake, *in vitro* cytocompatibility, *in vivo* pharmacokinetic profile, and pharmacodynamic study in NDEA induced HCC-bearing rats.

https://dx.doi.org/10.1021/acsbiomaterials.0c00429
ACS Biomater. Sci. Eng. XXXX, XXX, XXX−XXX

Table 1. Independent and Dependent Variables Used in the 3^2 Factorial Design Approach for Optimizing Liposomal Formulation[a]

Independent variables	levels			Dependent variables
	−1	0	+1	
molar ratio of SL/Chol	6:2	7:2	8:2	
concentration of SL and Chol (mg) based on molar ratio	343:57	350:50	357:43	vesicle size (VS), ζ potential (ZP), and encapsulation efficiency (EE)
concentration of SA (mg)	2.5	5.0	7.5	

[a]Concentrations of all the excipients are mentioned for the final batch of 20 mL with 20 mg of resveratrol (RS). SL, soya lecithin; Chol, cholesterol; SA, stearyl amine.

2. MATERIALS AND METHODS

2.1. Materials. RS (>98%) was supplied by M/s Sami Laboratories (Bangalore, India). Lipoid S100 soyalecithin (N94% phosphatidylcholine, SL) was provided by Lipoid GmbH, Ludwigshafen, Germany. Cholesterol (Chol) was purchased from Loba Chemie Pvt. Ltd., Mumbai, India. HPLC-grade acetonitrile was purchased from M/s Merck, Mumbai, India, and *N*-nitrosodiethylamine (NDEA-N0258), coumarin6 (442631), and stearylamine (SA-74750) were purchased from Sigma-Aldrich, Bangalore, India. Serum aspartate amino transferase (AST), serum alanine transaminase (ALT), alkaline phosphatase (ALP), total bilirubin (TB), total protein (TP), and γ-glutamyl transpeptidase (GGT) kits were purchased from ERBA Diagnostics Mannheim GmbH, Bangalore India. Rat α-fetoprotein (AFP) ELISA kit was purchased from Qayee-Biotechnology Co., Ltd., New Delhi, India. HepG2 cell lines and normal mouse fibroblasts were obtained from the National Centre of Cell Sciences, Pune, India. Fetal bovine serum (FBS), Pen-Strep (a mixture of streptomycin and penicillin), and Dulbecco's modified eagle medium (DMEM) were procured from HiMedia Laboratories Pvt. Ltd., Bangalore, India.

2.2. Preparation of Resveratrol Entrapped Cationic Liposomes. On the basis of preliminary studies, a 3^2 factorial approach (Design Expert Software (version 7, State-Ease Inc.) was used to optimize the RLs, in which the molar ratios of soya lecithin/cholesterol (SL/Chol) and SA were selected as independent variables. The mean vesicle size (VS), ζ potential (ZP), and encapsulation efficiency (EE) were selected as dependent variables (Table 1). The generated polynomial equation was used for the evaluation of the response,

$$Y = b_0 + b_1X_1 + b_2X_2 + b_{12}X_1X_2 + b_{11}X_1^2 + b_{22}X_2^2 \quad (1)$$

RLs were prepared by a thin film hydration method, as described by Bangham et al. in 1965.[32] Briefly, RS (20 mg), SA, SL, and Chol were solubilized in the mixture of organic solvent chloroform and methanol (2:1 v/v). The organic solvent was evaporated on rotavapor R-210 under reduced pressure (vacuum pump, V-700 Buchi) for 1 h at 40 °C to obtain a thin film. The film was then treated with a stream of nitrogen gas and kept in a vacuum overnight to remove any final traces of solvents. The lipid film was hydrated at 40 °C with 20 mL of phosphate buffer (pH 6.4) to aid in the formation of liposomes. Formulated RLs were sonicated for 2 min on an ice bath using a high intensity probe ultrasonic generator (Rivotek) with a probe diameter of 15 mm (15 s on/off pulse). Following sonication, the resulting liposome dispersion was centrifuged (Kubota 6500) at 2000 rpm at 4 °C for 10 min to separate the undissolved RS. RLs were then filtered five times using syringe filters (0.44 and 0.22 μm) successively to yield monodispersed RLs. Finally, cryoprotectant (mannitol 5% w/v) was added to RL dispersion and lyophilized (CHRIST Alpha 1−2 LD plus) for further studies. For lyophilization, the RL dispersion was frozen at −80 °C for 24 h, followed by freeze-drying for 48 h. The lyophilizer was set with −55 °C as the condenser temperature and 0.023 mbar as the vacuum pressure. The lyophilized formulation was evaluated for the appearance of the cake, reconstitution time, ZP, VS, and EE.[33]

2.3. Characterization of Liposomes. Dynamic light scattering (zetasizer Nano-ZS90, Malvern Instruments) was used to measure VS, PDI, and ZP of all RL formulations, and the surface morphology was analyzed by using a transmission electron microscope (TEM; Philips CM12 Electron Microscope). For TEM analysis, the aqueous dispersion of RL5 was stained with 1% phosphotungustic acid (sequential two-droplet method) and was visualized under TEM. For Fourier transform infrared spectroscopy (FT-IR, Shimadzu), each chemical components of the formulation and lyophilized RL were analyzed using a KBr pellet technique. For differential scanning colorimetry (DSC) studies, dried samples of raw material and optimized RLs were analyzed by using a DSC 823 instrument (Mettler Toledo,). Briefly, each sample (4−5 mg) was weighed, compressed into an aluminum pan, and scanned in the temperature range from 50 to 300 °C at a heating rate of 10 °C/min.

2.4. Estimation of Entrapment Efficiency (EE) and Drug Loading (DL). The EE of RLs was determined using an indirect method,[34] which involves measuring the amount of free drug available in nano dispersion. RL dispersion was centrifuged (Kubota 6500) at 2000 rpm (using rotor model AG-1212) at 4 °C for 10 min, and the supernatant was then separated. The pellet of the unentrapped drug (free drug) was determined by using a reverse-phase HPLC method.[13] The EE and DL[35] were calculated by the formulas shown below.

$$\text{percent EE} = \frac{(\text{WT} - \text{WF})}{\text{WT}} \times 100 \quad (2)$$

$$\text{percent DL} = \frac{\text{WR}}{\text{WL}} \times 100 \quad (3)$$

where WT is the weight of RS used for liposome formation, WFis the weight of unencapsulated RS, WR is the weight of RS in liposomes, and WL is the total weight of lipid and RS added in formulation.

2.5. *In Vitro* Drug Release and Release Kinetic Studies of RL. *In vitro* release of RS from liposomes was performed by ready-to-use dialysis tubes (Spectrum Laboratories, Rancho Dominguez, CA) having a MWCO of 12 400 Da, a pore size of <10 nm, and 10 cm length with a membrane diameter of 10 mm with a seal at one end and attached to a floatable cap. Release studies were performed in phosphate buffer saline (PBS) (pH 7.4- simulated blood pH) and PBS (pH 5.5- simulated tumor micro environment pH), both containing 0.1% v/v polyethylene glycol (PEG-400) to solubilize the released RS. Briefly, RL5 (5 mL equivalent to 4 mg RS) was transferred to dialysis bag, which was immersed into a 200 mL bottle containing 100 mL of PBS (pH 5.5 and 7.4). Bottles were placed on a magnetic stirrer pre-equilibrated at 37 ± 0.5 °C with a stirring speed of 100 rpm. At specific time intervals, the aliquots (0.5 mL) were withdrawn and replaced with an equal amount of fresh PBS. All aliquots were filtered by using a 0.45 μm syringe filter, and the amount of RS released was analyzed by HPLC.[36,37] In order to understand the drug release mechanism of optimized formulation (RL5), different kinetics models such as zero order, first order, Higuchi model, Korsmeyer -Peppas model, and Hixson Crowell model were evaluated. The best model was evaluated on the basis of the maximum value of the correlation coefficient (R^2).[36]

2.6. Stability Studies of RL. RL5 dispersion and lyophilized formulations were stored at 4 °C over a period of 3 months for stability studies. Both RL5 dispersion and lyophilized form were evaluated for VS, ZP, and EE for confirmation of stability.[33,38] After 3 months, the dispersion was centrifuged for 10 min at 2000 rpm and the supernatant liposomes were evaluated for the entrapped RS.

https://dx.doi.org/10.1021/acsbiomaterials.0c00429
ACS Biomater. Sci. Eng. XXXX, XXX, XXX−XXX

Table 2. Experimental Groups Used in the Study to Evaluate the Effect of Prophylactic and Therapeutic Treatment in HCC Induced Rats[a]

Group I (normal group)	rats fed with standard diet and were administered with vehicle (a mixture of 1% DMSO and 1% Tween 80 in PBS) twice a week.
Group II (disease control)	NDEA (carcinogen) intragastric administration until the 12th week
	prophylactic treatment
Group III received RS	NDEA administration until 12th week + simultaneous intraperitoneal dosing of RS (20 mg/kg body weight/twice a week)
Group IV received RL5	NDEA administration until 12th week + simultaneous intraperitoneal dosing of RL5 (equivalent to RS 20 mg/kg body weight/twice a week)
	therapeutic treatment
Group V received RS	NDEA administration until 12th week + intraperitoneal dosing of RS (20 mg/kg body weight/twice a week) starting from 9th week
Group VI received RL5	NDEA administration until 12th week + intraperitoneal dosing of RL5 (equivalent to RS 20 mg/kg body weight/twice a week) starting from 9th week

[a]Note: RS, resveratrol; RL5, optimized RS loaded liposomes; NDEA, *N*-nitrosodiethylamine.

Liposomes were dissolved in chloroform and methanol mixture to solubilize the lipids and RS. The solution was then diluted with acetonitrile (a component of HPLC solvent system), followed by centrifugation and filtration by using syringe filter (0.45 μm) for HPLC analysis.

2.7. *In Vitro* Biocompatibility Studies. *2.7.1. Blood Compatibility (Hemolysis Assay).* The blood biocompatibility of RL5 was confirmed by an erythrocyte lysis test.[39] Fresh blood was collected into the heparinized tubes from rats and centrifuged at 2500 rpm for 10 min at 4 °C for separation of red blood cells. The pellet was washed thrice with PBS and then finally resuspended in PBS and used for hemolysis assay. An equal volume (1 mL) of erythrocyte suspension and liposomal dispersion was mixed and incubated for 1 h at 37 °C under constant shaking. After 1 h, the mixture was subjected to centrifugation and the supernatant was analyzed at 540 nm for percent hemolysis using an UV−vis spectrophotometer (UV-1800 Shimadzu Corporation, Kyoto, Japan). The separated supernatant from the centrifuged blood sample was considered as blank and supernatant derived from the blood sample treated with 1% Triton w/v (hemolytic agent) was taken as the positive control. The experiments were performed in triplicates, and the percent hemolysis was calculated by using formula shown below:

$$\text{percent hemolysis} = \frac{\text{TA} - \text{BA}}{\text{PCA} - \text{BA}} \times 100 \quad (4)$$

where TA is test absorbance, BA is blank absorbance, and PCA is positive control absorbance.

2.7.2. Cytocompatibility Assay. The cytocompatible behavior of RS and RL5 was assessed using standard MTT (3-(4,5-dimethylthiazol-2-yl)-2,5-diphenyltetrazolium bromide) assay. Briefly, normal mouse fibroblasts (L929) cell lines were grown in a mixture of Dulbecco's modified eagle medium (DMEM), fetal bovine serum (FBS, 10%), and Pen-Step antibiotics (1%) in a CO_2 incubator (Eppendorf, New Brunswick, Galaxy 170R) at 37 °C with 95% humidity. Seeding of L929 cell lines at the densities of 1×10^4 cells/well in the 96 well plate was carried out, and the plates were incubated for 24 h in a CO_2 incubator to allow for cell adhesion. The media was discarded and swapped with fresh media with varying concentrations of RS and RL5 (250, 125, 62.5, 31.25, 15.63, and 7.81 μg/mL), and the control wells were treated with equivalent volumes of media without any test compound, followed by incubation for a period of 24 h. After the completion of the incubation period, the media in each well was discarded and wells were gently washed with PBS. Cells were then treated with 100 μL of MTT solution (0.5 mg/mL in phosphate buffer saline), and the plate was incubated at 37 °C for 4 h. After 4 h, the supernatant was discarded and DMSO (100 μL) was added to each well to dissolve formed formazan crystals and analyzed by plate reader (Lisa plus) to calculate the percent cell viability.[40,41]

2.8. *In Vitro* Cytotoxicity Assay. The cytotoxicity of RS and RL5 against HepG2 cell lines was performed as per the procedure mentioned in section 2.7.2. HepG2 cell lines were incubated with RS and RL5 of varying concentrations (250, 125, 62.5, 31.25, 15.63, and 7.81 μg/mL) equivalent to free RS for 24 and 48 h. After completion of the incubation period, percent cell viability was estimated by MTT assay method.

2.9. Quantitative and Qualitative Cell Uptake Assay. For qualitative cell uptake analysis, coumarin 6 (C6) was used as a model fluorescent dye to evaluate the extent of cellular uptake of liposomes. HepG2 cells were seeded in 6-well culture plates (50 000/well) and were incubated overnight for the attachment of the cells. The efficacy of cellular uptake as a function of RL5 was evaluated by *in vitro* incubation of HepG2 cells with free C6 and C6 loaded liposomes (CLs) (equivalent to 1 μg/mL C6) for 3 and 5 h.[42] The free C6 solution was prepared by solubilizing in 0.1% DMSO to yield a final concentration of 1 μg/mL.[43] CLs were prepared by following the method mentioned in section 2.2 and replacing RS with C6. After the given time of incubation of C6 and CL, the medium was aspirated and cells were washed with PBS five times, fixed with 4% paraformaldehyde (Merck), and were observed under a confocal laser scanning microscope (CLSM) (Olympus FV1000). For quantitative cell uptake analysis, HepG2 cells were treated with RS and RL5 (equivalent to 10 μg/mL RS) and further incubated for 3 and 5 h to determine cell uptake over time. Media was removed, and cells were washed thrice with PBS and then lysed with 0.1% Triton X-100. Lysed cells were then extracted with ACN for the complete dissolution of internalized RS. Finally, the cell lysate was centrifuged at 10 000 rpm for 10 min and supernatant was analyzed by HPLC.[42]

2.10. *In Vivo* Organ Toxicity Studies. Biochemical parameters of hepatic and renal functions such as alanine transaminase (ALT), aspartate transaminase (AST), blood urea nitrogen (BUN), and creatinine were assessed by commercially available diagnostic kits (Erba Diagnostics, Inc.). Organs such as liver, kidney, and spleen tissues of rats were stained with hematoxylin and eosin (H&E) for histopathological assessments.

2.11. Pharmacokinetic Study and Hepatic Accumulation of RS by HPLC. Animal studies were approved by the Institutional Animal Ethical Committee (KLECOP/IAEC/Res.22-10/10/2015), KLE College of Pharmacy, Belagavi, India. Studies involving animals were conducted in strict accordance with Animal Research: Reporting of *In Vivo* Experiments (ARRIVE) guidelines.[44] For *in vivo* pharmacokinetic study, male Wistar albino rats (200 ± 20 g) were obtained from our institution's animal housing facility and were housed in cages at room temperature 25 ± 2 °C and relative humidity of 50−60% under a 12 h light/dark cycle. Rats were fed with a pellet diet (VRK Nutritional Solutions, Pune, Maharashtra, India), with water, *ad libitum* for 1 week before experiments. NDEA was used to induce HCC in 6−7 week old healthy male rats. NDEA solution reconstituted in saline was administered intragastrically at a dose of 10 mg/kg body weight with the frequency of 5 times a week for 12 weeks.[45] HCC induced animals were randomly divided in two groups (n = 3 for each time point) and were administered with 20 mg/kg body weight of RS and equivalent RL5. Free RS was solubilized in a mixture of 1% DMSO and 1% Tween-80 solution in phosphate buffer saline (PBS).[46] On the basis of the permissible limit (less than 10 mL) for intraperitoneal injection,[47] the injection volume was kept around 1 mL considering the weight of the rats. Experimental rats were anaesthetized, and blood samples (1 mL) were collected in

https://dx.doi.org/10.1021/acsbiomaterials.0c00429
ACS Biomater. Sci. Eng. XXXX, XXX, XXX−XXX

Table 3. Observed Responses from 3^2 Factorial Design of Resveratrol Loaded Liposomes[a]

	independent variable		dependent variable			
formulation code	A	B	EE (%)	VS (nm)	ZP (mV)	DL (%)
RL1	−1	−1	49.26 ± 9.72	153.33 ± 7.50	07.57 ± 3.66	2.38 ± 0.45
RL2	−1	0	62.57 ± 7.45	140.30 ± 10.16	25.98 ± 5.82	2.99 ± 0.34
RL3	−1	1	58.91 ± 7.06	134.73 ± 5.09	29.26 ± 7.40	2.80 ± 0.32
RL4	0	−1	62.76 ± 6.17	176.43 ± 7.16	15.88 ± 4.27	3.02 ± 0.28
RL5	**0**	**0**	**78.14 ± 8.04**	**145.78 ± 9.9**	**38.03 ± 9.12**	**3.71 ± 0.36**
RL6	0	1	65.31 ± 5.59	138.18 ± 12.35	62.58 ± 4.13	3.10 ± 0.26
RL7	1	−1	63.65 ± 4.63	187.54 ± 7.29	11.73 ± 2.58	3.06 ± 0.21
RL8	1	0	70.74 ± 5.99	152.46 ± 7.52	35.00 ± 7.04	3.33 ± 0.25
RL9	1	1	65.85 ± 7.54	148.91 ± 7.27	56.43 ± 9.14	3.12 ± 0.34

[a]Note: (A) molar ratio of SL/Chol, (B) concentration of SA (mg). Each value represents the mean ± SD, $n = 3$. The composition of each batch is given in Table 1. The optimized values are represented in bold.

heparinized tubes *via* cardiac puncture at 15, 30, 60, and 120 min and sacrificed by cervical dislocation. Major organs such as heart, spleen, liver, lung, and kidney were excised, washed twice with ringer's solution, and immediately frozen until analysis. Isolated organs were weighed, minced thoroughly, and homogenized (RQT-127AD, Remi Elektrotechnik Ltd., Vasai, India) in 50% aqueous acetonitrile. Homogenized samples were centrifuged (12 000 rpm for 12 min), and the supernatant was preserved at −20 °C for further analysis. For estimation of RS in rat plasma, blood samples were centrifuged at 4000 rpm for 10 min at 4 °C for plasma separation and were preserved at −20 °C for further sample analysis. RS from frozen isolated organs and plasma were estimated by using a modified HPLC method.[48] Separated biological samples from both tissue homogenate and plasma (150 μL) were vortex-mixed with 150 μL of ACN for deproteinization, followed by centrifugation at 12 000 rpm for 12 min. Supernatants were separated, filtered through 0.22 μm membrane filter (Millipore), and finally analyzed by the HPLC system. The pharmacokinetic investigation was performed by one compartmental model using Kinetica software (Thermo-Scientific) to estimate the parameters such as area under curve (AUC), peak plasma concentration (Cmax), half-life ($t_{1/2}$), and mean residence time (MRT).[49]

2.12. Pharmacodynamics Activity: Prophylactic and Therapeutic Anti-Cancer Activity. The experimental animals were divided into six groups (Table 2) with six animals in each group. Group 2 (NDEA induced HCC rats: disease control) consisted of two more rats to ensure the successful generation of HCC at the end of the ninth week of the experiment. At the 13th week, rats in each group were sacrificed and liver specimens were removed and weighed. Plasma was collected from the blood by centrifugation at 4000 rpm for 10 min at 4 °C for biochemical estimation of alanine transaminase (ALT), alkaline phosphatase (ALP), aspartate transaminase (AST), total bilirubin levels, γ-glutamyl transpeptidase (GGT), and α-fetoprotein (AFP). After dissection, the liver was isolated and the tumor nodules were counted and stored in buffered formalin for histopathological examination.

3. RESULT AND DISCUSSION

3.1. Formulation and Optimization of RS Loaded Cationic Liposomes. Physicochemical properties and stability are the key factors to be considered while developing a new drug delivery system in all the formulation stage, especially those proposed for parenteral administration. In the present investigation, the RLs obtained from the 3^2 factorial design confirmed that the independent variables such as (A) the molar ratio of SL/Chol and (B) the concentration of SA had a significant effect on dependent variables such as EE, VS, and ZP (Table 3). The quadratic equation generated from Design-Expert Software (Stat-Ease Inc., Minneapolis, MN) for EE is

$$EE = 75.09 + 4.92A + 2.40B - 1.86AB - 6.91A^2 - 9.53B^2 \quad (5)$$

The positive sign indicates that EE is directly proportional to both the independent variables. The literature reveals that the increase in the concentration of SL subsequently increases EE, the reason for which could be attributed to the fact that lipophilic drugs like RS tend to easily dissolve in lipid resulting in a higher EE.[50] SA at the same time alters the membrane permeability or the electric charge density, resulting in enhanced EE of the liposomes.[51]

$$VS = 145.46 + 10.25A - 15.32B - 6.40AB - 0.38A^2 + 9.92B^2 \quad (6)$$

where the positive sign indicates that VS is directly proportional to A (molar ratio of SL/Chol) and the negative sign indicates inversely proportional to B (concentration of SA). The reduction in the VS could be due to the ability of SA to generate a net positive charge on the surface of RLs. An increase in the surface charge increases the intervesicular Brownian moment, keeping the particles stable. It also avoids the ripening of vesicles over time, which could be a key reason for a smaller VS.[52,53] The equation further advocates that VS was directly proportional to the concentration of SL, for which the reason could be attributed to the propensity of SL molecules to coalescence, leading to an increase in VS.[54] Hence, an optimum concentration of SL and SA is a prime requirement to obtain stable monodisperse nanoliposomes.

$$ZP = 38.53 + 5.36A + 20.41B + 3.40AB - 9.84A^2 + 1.05B^2 \quad (7)$$

All the formulations were analyzed for ZP as a part of the formulation development process. ZP is a useful tool to indicate the vesicle surface charge, which is used to predict the stability of colloidal dispersion. In general, ZP is the balance between the surface positive and negative charges and is directly proportional to the magnitude of the potential.[55] On the basis of the result, the positive sign indicates that the ZP is directly proportional to A and B. Our experiments were supported by the literature, which states that an increase in the concentration of SA consequently increases the ZP. In the present investigation, the ZP in all the formulations was maintained on the positive side, owing to the charge imparted by SA. Cationic lipid SA is an amphiphilic molecule, which has a lipophilic region (hydrocarbon chain) and a hydrophilic

https://dx.doi.org/10.1021/acsbiomaterials.0c00429
ACS Biomater. Sci. Eng. XXXX, XXX, XXX−XXX

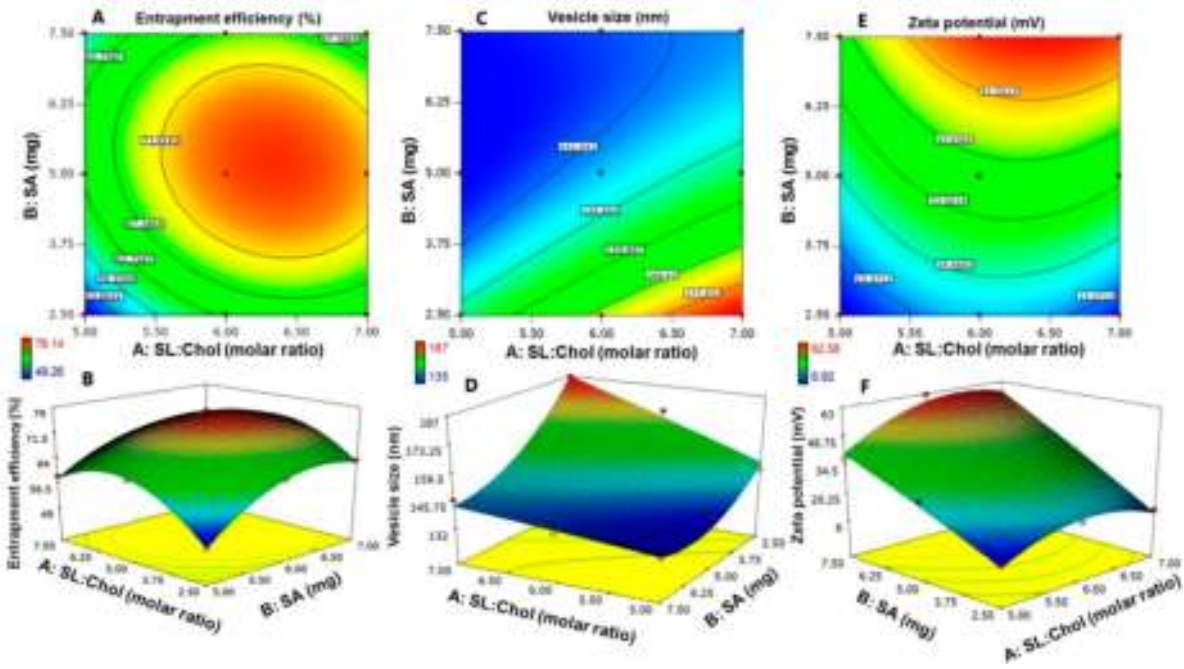

Figure 2. 2D contour and 3D response plots (design expert software) for (A and B) entrapment efficiency, (C and D) vesicle size, and (E and F) ζ potential, respectively. The 3^2 level factorial design demonstrated the significant influence of lipid and cholesterol molar ratio and stearyl amine concentration on ζ potential, vesicle size, and encapsulation efficiency. SL, soya lecithin; Chol, cholesterol; SA, stearyl amine.

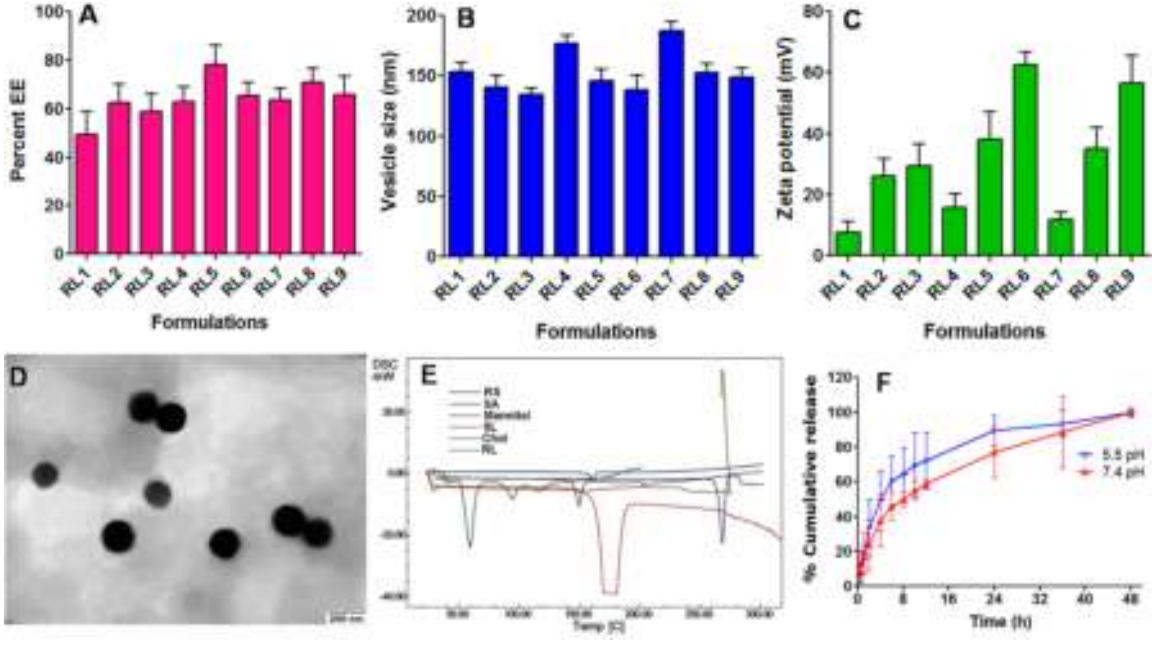

Figure 3. (A) Percent entrapment efficiency of RL1−RL9 by varying the ratio of SL/Chol. On the basis of the design of experiments, RL5 formulation was selected, owing to its highest EE for further *in vitro* cell uptake and animal study. (B) Graph showing the hydrodynamic diameters of RL1−RL9 in deionized water at pH 7.0. The figure shows that all formulations were in the range 134.73 ± 5.09−187.54 ± 7.29 nm, from which the optimized formulation RL5 was found to be 145.78 ± 9.9 nm in diameter. (C) Bar graph showing the ζ potential of RL1−RL9 in deionized water at pH 7.0. All formulations were in the range 7.57 ± 3.66−62.58 ± 4.13 mV, from which the optimized formulation RL5 was found to be 38.03 ± 9.12 mV, representing a stable RL dispersion. (D) Surface morphology of RL5 was confirmed and determined by TEM, which clearly showed spherical morphology with uniform size distribution. (E) DSC thermogram of RS, exhibiting a sharp endotherm at 256.45 °C, indicating its melting point, and conforming its crystalline nature, whereas SA, Chol, mannitol, and soya lecithin exhibited sharp endotherm peaks at 52, 149, 166.0, and 20.5 °C, respectively, corresponding to their melting points. The endotherm peak almost disappeared in the thermogram of RL5, suggesting that RS was entrapped in liposomes. RL5 shows clear peak of mannitol at 166.0 °C, which corresponds to crystallized mannitol. (F) *In vitro* drug release of RS from RL5 at pH 5.5 and 7.4 showed a faster release trend pH 5.5 when compared to pH 7.4. SL, soya lecithin; Chol, cholesterol; SA, stearyl amine, RL, resveratrol loaded cationic liposomes.

https://dx.doi.org/10.1021/acsbiomaterials.0c00429
ACS Biomater. Sci. Eng. XXXX, XXX, XXX−XXX

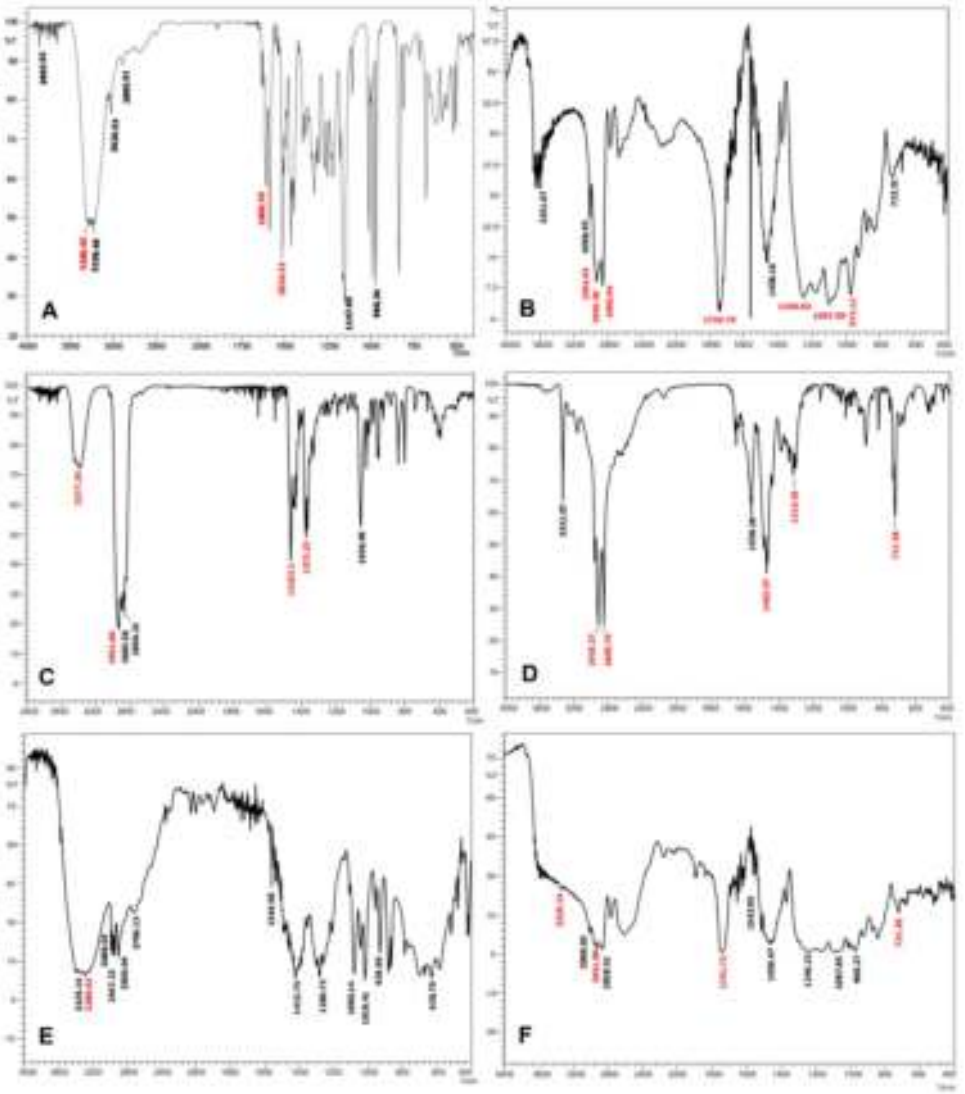

Figure 4. (A) FT-IR spectrum of RS, which revealed the intense absorption band of phenolic hydroxyl group at 3288 cm^{-1}, benzene ring absorption peaks of C═C at 1606 cm^{-1}, and medium absorption peak at 1514 cm^{-1}. (B) FT-IR spectrum of SL (LIPOID S100), in which characteristic peaks at 2954 cm^{-1} (hydroxyl stretching), 2900 and 2856 cm^{-1} (C—H stretching of long fatty acid chain), 1739 cm^{-1} (carbonyl stretching of the fatty acid ester), 1246 cm^{-1} (P═O stretching band), 1097 cm^{-1} (P—O—C stretching), and 972 cm^{-1} $(N^{+}(CH_3)_3$ stretching were observed. (C) FT-IR spectrum of Chol displayed a characteristic band between 2866−2931 cm^{-1} representing asymmetric and symmetric stretching vibrations of CH_2 and CH_3 groups and a broad and intense band nearly at 3377.36 cm^{-1} due to —OH stretching. The additional bands at 1463 and 1375 cm^{-1} is due to asymmetric stretching vibrations and bending vibration of —CH_2 and —CH_3 groups. (D) FT-IR spectrum of SA showed peaks at 2916 and 2850 cm^{-1}, owing to —C—H stretching, and 1463 cm^{-1}, owing to —N—H bending. Further, a sharp peak at 1315 cm^{-1} could be attributed to C—N stretching and a peak at 721 cm^{-1} represents —N—H wagging vibration. (E) FT-IR spectra of mannitol showed a broad characteristic peak at 3280 cm^{-1} assigned to the hydroxyl group. (F) FT-IR spectra of lyophilized RL5 showed characteristics peaks of mannitol, Chol, and SA but did not show any characteristics peaks of RS, which indicates the complete entrapment of RS inside the liposomes.

region comprising a positively charged polar amine group. The previous reported literature by Casals et al., clearly shows that SA is asymmetrically distributed in the lipid bilayer, which was predominantly on the outer surface as compared to the inner core. A high positive ζ potential value of the formulated liposomes confirms that a significant SA is available on the outer surface, imparting the cationic charge on the liposomes.[56,57] The application of ANOVA (Table S1) on the outcomes confirms the significance of the model from F and P values. The surface response curve and contour plots (Figure 2) reveal the effect of SL and SA on EE, VS, and ZP. The evaluation of liposomes suggested that RL5 demonstrated desirable properties, i.e., more than 78% EE, ZP of 38 mV, and the VS of less than 150 nm when compared with other formulations. Finally, the optimized liposomes RL5 were lyophilized by using cryoprotectant mannitol. The lyophilized RL5 cake was found to be intact and fluffy in nature with a reconstitution time less than 35 s.

3.1.1. Evaluation of Optimized Liposomes Formulation. VS, ZP, PDI, and EE of optimized liposomal formulation RL5 were found to be 145.78 ± 9.9 nm, 38.03 ± 9.12 mV, 0.359 ± 0.03, and 78.14 ± 8.04% (Figure 3A−C) respectively. Results revealed that VS, EE, and ZP values of liposomes were directly related to the concentration of SL and SA used in the formulation. The morphological examination of liposomes evaluated by TEM clearly showed a spherical morphology with

https://dx.doi.org/10.1021/acsbiomaterials.0c00429
ACS Biomater. Sci. Eng. XXXX, XXX, XXX−XXX

Table 4. Stability Studies of Optimized Liposomes RL5[a]

parameter →	vesicle size (nm)		ζ potential (mV)		EE (%)	
storage condition ↓	initial	after 3 months	initial	after 3 months	initial	after 3 months
RL5, liquid dispersion at 4 °C	142.17 ± 6.20	149.14 ± 12.62	37.3 ± 4.53	34.43 ± 4.80	76.57 ± 2.51	72.77 ± 3.05
RL5, lyophilized at 4 °C	143.76 ± 4.77	147.80 ± 10.30	36.66 ± 2.65	35.03 ± 3.27	76.44 ± 2.27	75.36 ± 0.929

[a]The data is expressed as mean ± SD (n = 3). The data were evaluated by Student's paired t-test, which showed no significant difference.

an uniform size distribution (Figure 3D) of vesicles. The reason for the formation of spherical morphology could be due to the hydrophobic nature of the lipids, which, when exposed to an aqueous environment, led to the spontaneous formation of closed bilayers, exposing the polar hydrophilic layer to the outer surface of liposomes. The shape and surface morphology of the liposomes was found to be smooth with no vesicular aggregation, which indicates the stability of the prepared liposomes.

DSC thermograms of RS, SL, SA, Chol, mannitol, and freeze-dried RL5 are shown in Figure 3E. The DSC thermogram of RS exhibited a sharp endotherm at 256.45 °C, which indicates the crystalline state of RS and confirms its melting point. The melting peak almost disappeared in the thermogram of RL5, suggesting that RS was entrapped in liposomes and the formulation changed from the crystalline state to the amorphous state. The DSC of pure SL exhibited endothermic peaks at 20.5 °C, indicating the transition temperature (Tm), which served as the basis for optimizing the temperature required for the film formulation of lipids. Further, SA and Chol thermograms showed strong endotherms at 52 and 149 °C, corresponding to their melting points, respectively, confirming their purity. These peaks were however not observed in the thermograms of RL5, which signifies the interaction between RS and other lipid components of the bilayer. RL5, however, shows a clear peak of mannitol at 166.0 °C, which was used as a cryoprotectant for lyophilization.

FT-IR spectroscopic studies were performed to analyze the drug and polymer/excipients interaction. The FT-IR spectra of lyophilized RL showed characteristics peak of mannitol but did not show any characteristics peaks of RS, which indicates the complete entrapment of RS inside the liposomes (Figure 4). The clear peak of amine groups at 1450 cm^{-1} in the FT-IR spectra of lyophilized RL5 could be attributed to the coating of SA onto the liposomes.

3.2. *In Vitro* Release Study of RL5. *In vitro* drug release profiles of RS from RL5 at pH 5.5 and 7.4 were obtained by plotting the graph of cumulative percentage of the drug released over time (Figure 3F). During the release study, 0.1% (v/v) of PEG was added in release medium PBS (pH 5.5 and 7.4) to solubilize the released RS. Initially, a burst release phase, releasing approximately 30% of resveratrol in both pH medium was observed in the first 2 h, followed by sustained and complete drug release in 48 h. No significant difference was found for the release of RS from RLs over the entire study period. A comparative faster release of RS at pH 5.5 (tumor microenvironment) could be due to use of heterogeneous lipids (SL and SA) used in the formulation of liposomes. SL (Lipoid S 100: lipid mixture)[58] and SA have an 18 carbon chain as their backbone. Liposomes prepared with heterogeneous lipids when exposed to a decreased pH lead to an increase in the membrane permeability and ultimately released the payloads. Our results are in corroboration with the studies performed by Karve et al., wherein they assessed the release behavior of vesicles formulated by different sets of lipids (DPPC (16 carbon containing lipid; 1,2-dipalmitoyl-*sn*-glycero-3-phosphocholine,) and DSPA (18 carbon containing; 1,2-distearoyl-*sn*-glycero-3-phosphate, sodium salt) lipids, DPPC and DPPA lipids, and DSPC and DSPA lipids) in different pH. Vesicles prepared with different chain lengths (DPPC and DSPA) showed an increased membrane permeability and higher release of encapsulated calcein at a lower pH when compared to the vesicles prepared by lipids with same chain length (DPPC−DPPA and DSPC−DSPA).[59] The drug release mechanism can be defined as the way of the release of payload from the nanocarrier. It is dependent of the nature of the polymer/lipid used in the formulation and the release conditions, which can follow several mechanisms such as dissolution, diffusion, swelling, erosion, and degradation.[36]

To examine the release mechanism of RS from the RL5, five kinetic models were applied to fit the release data. On the basis of the analysis (Figure S1A−E), the Hixson−Crowell model showed the highest R^2 value for RL5 at pH 5.5 (R^2 value: 0.937) and 7.4 (R^2 value: 0.971). Hence, the release of RS from RL5 follows the Hixson−Crowell model, which occurs through surface dissolution and is dependent on the surface area and the diameter of vesicle.[60,61]

3.3. Stability Studies. Physical stability of liposomes is indirectly proportional to the vesicle size and directly proportional to the ζ potential of the dispersion. Aggregation of vesicles, which represents poor stability, could be observed during formulation processing and/or upon storage. The increase in the diameter of liposomes results in a rapid uptake by the reticuloendothelial system with subsequent clearance, resulting in a short half-life. Therefore, preparing stable liposomes with small and uniform size distribution is the most significant aspect in drug product development. Table 4 represents the storage stability studies conducted for optimized RL5 after storage at 4 °C for 3 months in both dispersion and lyophilized forms (reconstituted with water). After 3 months of storage at 4 °C, there was no significant difference in the VS, ZP, and EE, which indicates a desirable stability of the formulation.

3.4. *In Vitro* Biocompatibility Studies. *3.4.1. Blood Compatibility (Hemolysis Assay) Studies.* Outlining the mechanism of liposomal interaction with red blood cells (RBCs) is an important step toward establishing the plausibility of using liposomes as delivery tools for biomedical applications. Formulations are expected to be inert and biocompatible with cells, blood, and blood components. In the present investigation, RL5 formulation (equivalent to 20 mg/mL RS) and free RS (20 mg/mL) were evaluated for hemolysis as compared to positive control (1% w/v Triton in PBS) and negative control (0.1% v/v DMSO in PBS), as depicted in Figure S2. Percent hemolysis values below 10% were considered to be nonhemolytic.[62] It was observed that formulated cationic RL5 caused 1.88% hemolysis, which is under the permissible limit (less than 10% lysis). Hemolysis assay suggests that the concentration of SA used in the

https://dx.doi.org/10.1021/acsbiomaterials.0c00429
ACS Biomater. Sci. Eng. XXXX, XXX, XXX−XXX

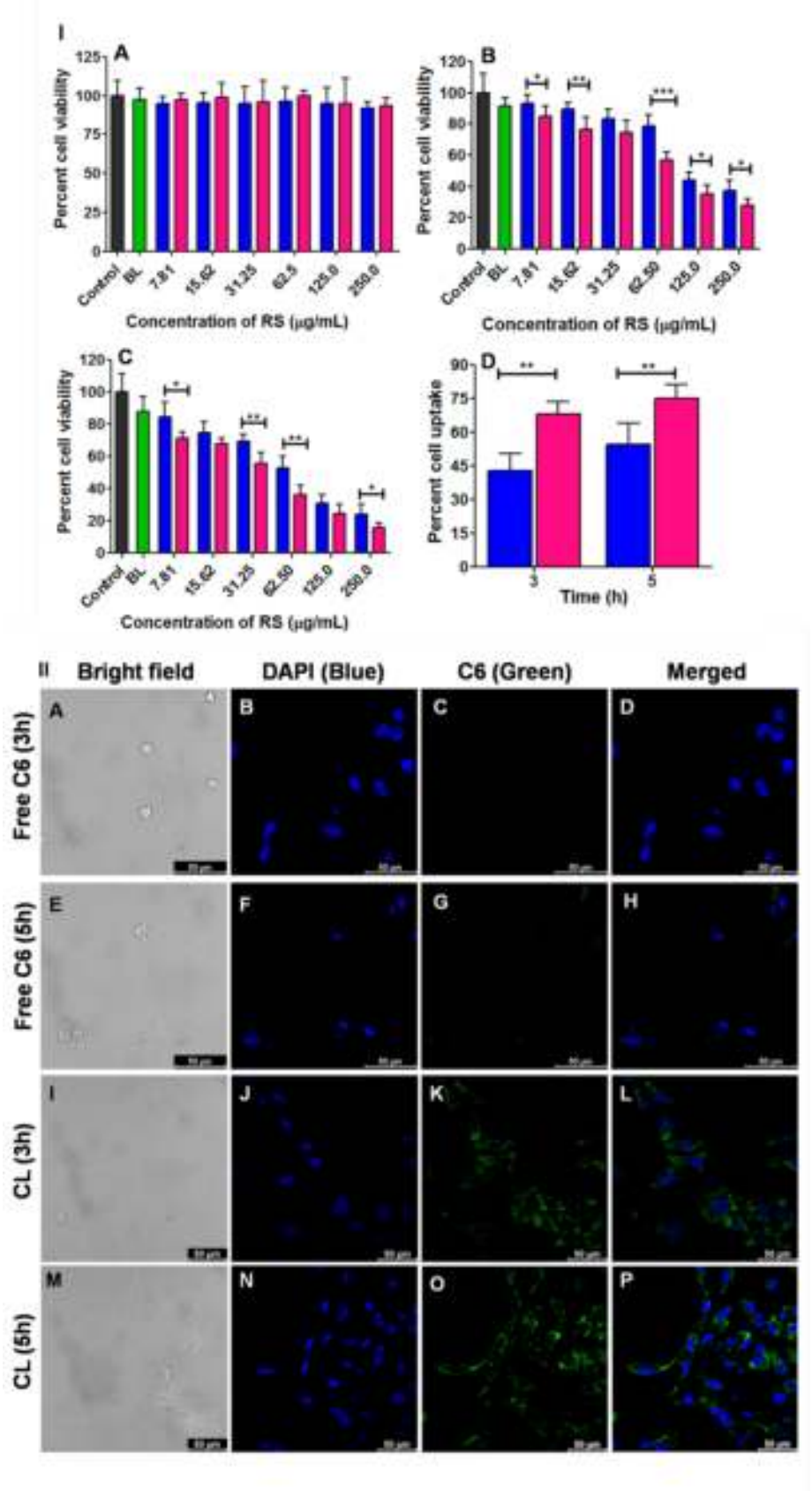

Figure 5. (I)(A) Cytocompatibility of RS and RL5 determined by evaluating the cytotoxicity against normal mouse fibroblast cell lines (L929) using colorimetric MTT assay. RS and RL5 were found to be biocompatible at the concentration range 7.812−250 μg/mL. (B and C) Graph showing cytotoxicity studies of BL, RS, and RL5 on HepG2 cell lines over a period of 24 and 48 h, and cell viability was estimated by MTT assay at different drug concentrations. BL were found to be biocompatible and showed no significant cytotoxicity against HepG2, whereas RS and RL5 showed dose- and time-dependent changes in which RL5 demonstrated a significantly higher cytotoxicity against HepG2 compared to that of RS.

https://dx.doi.org/10.1021/acsbiomaterials.0c00429
ACS Biomater. Sci. Eng. XXXX, XXX, XXX−XXX

Figure 5. continued

The half-maximal inhibitory concentration (IC50) values of RS after 24 and 48 h of incubation were 84.49 and 68.23 μg/mL and for RL5 were 63.65 and 42.26 μg/mL, respectively. (D) Bar graph showing quantitative cell internalization of RS and RL5 in HepG2 cancer cells, which were evaluated at 3 and 5 h time points by HPLC. The time-dependent cellular uptake showed augmented cellular internalization of RL5 as compared to RS throughout the incubation time ($p < 0.05$). Results demonstrated 54.16 ± 9.61 and 74.98 ± 6.33% cellular internalization after 5 h of incubation with RS and RL5, respectively. (II) Qualitative cell uptake study of C6 and CL showing time-dependent cellular uptake, wherein a higher uptake of CL by HepG2 was observed as compared to that free C6 at 3 (A−D and I−L) and 5 h (E−H and M−P). Scale bar is 50 μm.

formulation of RL5 is blood biocompatible and can be used for *in vivo* administration.

3.4.2. Cytocompatibility Assay. Cytocompatibility is the key parameter to be assessed for any bionanomaterial proposed for *in vivo* drug delivery system. In the present investigation, the cytocompatibility of RS and RL5 was evaluated against primary mouse fibroblast culture (L929) using colorimetric MTT assay. Cytotoxicity of samples was compared with control (untreated) cells that were considered as 100% viable (Figure 5IA). Fibroblast cells were treated with RS and RL5 at varying concentrations of 250, 125, 62.5, 31.25, 15.62, and 7.812 μg/mL and were evaluated for cell viability after 24 h. Both RS and RLs showed no significant difference in cell viability, which confirms its cytocompatibility.

3.5. Cytotoxicity Assay. Cytotoxicity studies of blank liposomes, free RS, and RL5 were tested on a HepG2 cell line over a period of 24 and 48 h using MTT viability assay at different drug concentrations (Figure 5IB,C). The half-maximal inhibitory concentration (IC50) was calculated by using Graph Pad Prism version 7.0, which signifies a quantitative measure of the concentration of a drug required to inhibit a given biological process by half. Blank liposomes were found to be biocompatible and showed no significant cytotoxicity against HepG2 when compared to control. RS and RL5 showed dose- and time-dependent changes in which RL5 demonstrated a significantly higher cytotoxicity against HepG2 when compared to RS. The IC50 of RS and RL after 24 h of exposure were found to be 84.49 and 63.65 μg/mL, respectively. After 48 h of incubation, the IC50 values of RS and RL were 68.23 and 42.26 μg/mL, respectively. Our results are in corroboration with the studies performed by Su et al., which showed that the IC50 values of free RS were around 68.4 and 34.2 μg/mL after 48 and 72 h, respectively.[63] The reason for improved activity and lower IC50 of RL5 in comparison to those of RS could be because of the enhanced uptake of liposomes and improved solubility of RS in nanoliposomes formulation.[64] Further, the negative charge on hepatocytes is more likely to attract positively charged liposomes, which increases the cell uptake of nanovesicles.[65,66] Similar outcomes were reported by De et al., wherein they developed SA based camptothecin loaded cationic liposomes. They reported that camptothecin loaded cationic liposomes demonstrated a manifold enhancement in the anti-cancer therapeutic efficacy both *in vivo* and *in vitro* in comparison with free camptothecin. This enhanced anti-cancer effect of liposomes was due to the attraction between the SA containing cationic liposomes toward the exposed PS group present on liver cancer cells.[67]

3.6. Qualitative and Quantitative Cell Uptake Assay. Cellular uptake efficiency was evaluated quantitatively by HPLC and qualitatively by CLSM. The cellular uptake showed an enhanced cellular internalization of RL5 as compared to that of RS throughout the incubation time ($P < 0.01$). HPLC analysis of cell extract after 5 h showed 54.16 ± 9.61 and 74.98 ± 6.33% cellular internalization of RS and RL5, respectively (Figure 5ID). By intending to evaluate the cellular internalization of developed liposomes, we developed CL and evaluated it using CSLM. C6 is a derivative of coumarin and is obtained from the plant origin. Owing to its fluorescent and lipophilic nature, it is used as a model fluorescent agent to qualitatively check the internalization of developed liposomes *via* fluorescence in both *in vitro* or *in vivo* experimental systems.[68] In our research investigation, CLSM results confirm that the HepG2 cells demonstrated a higher uptake of CL as compared to free C6, which was evident from confocal images of cells after 3 and 5 h of incubation (Figure 5IIL,P). An intense green fluorescence of CL was observed around the nucleus within the cytoplasm of HepG2 cells, whereas free C6 demonstrated a weak fluorescence signal (Figure 5IIC,G). Upon incubation of CL with HepG2 cells, the increased fluorescence intensity in the HepG2 cell membrane could be due to the accumulation of CL into the lysosomal compartment along with diffusion into the cytoplasm. Similar results were demonstrated by Parvathaneni et al., in which free C6 showed a reduced cell internalization than its corresponding CL.[69] This difference could be attributed to the relatively enhanced lipophilic nature of CL than C6. Out of the several reasons, lipophilic nature, solubility of test compound, and the time of incubation with cells are the key factors determining the uptake of the compound by cells. The literature suggests that C6, when suspended in aqueous media, is known to have a lesser uptake when compared with that of C6 solubilized in DMSO. This means that solubility of the compound is directly proportional to the cell uptake.[70,71]

Cationic nanoparticles with a net positive surface charge emerge as a promising option owing to their very strong cellular interaction and desirable cellular uptake.[30] As explained above, apart from PS on the surface of cancerous cells, it also contains strong negatively charged elements such as chorionic gonadotropin, sialic acid, and anionic residues of RNA as compared to normal cell surfaces.[72,73] On the basis of this fundamental electrostatic interaction, cationic liposomes have a high tendency to accumulate in cancer cells through endocytosis.[72]

3.7. *In Vivo* Toxicity Studies. The toxicity profiling of RS and RL5 were carried out using different toxicity markers. BUN, and plasma creatinine levels were determined for evaluating nephrotoxicity, while plasma ALT and AST levels were determined for evaluating the hepatotoxicity. Untreated animals served as the control for the comparison. As shown in Figure S3I, animals treated with RS and RL5 did not induce toxicity in the liver, spleen, and kidneys. The biochemical evaluation was further corroborated with histopathological examinations, suggesting a nontoxic behavior of free RS and RL5. Histological sections of liver, kidney, and spleen (Figure S3II) demonstrated normal parenchymal cell physiology, indicating no signs of inflammation and necrosis.

https://dx.doi.org/10.1021/acsbiomaterials.0c00429
ACS Biomater. Sci. Eng. XXXX, XXX, XXX−XXX

Table 5. Pharmacokinetic Parameters of RS and RL5 in Rat Plasma and Organs Following ip Administration

parameters		C_{max}	AUC_{total} (μg/mL·min)	$T_{1/2}$ (min)	MRT (min)
blood	RL5	2.15	225.98	56.24	95.70
	RS	1.74	125.06	48.86	83.58
liver	RL5	3.51	223.54	35.75	72.16
	RS	1.50	69.85	37.36	58.29
spleen	RL5	2.83	74.32	18.92	40.99
	RS	2.50	113.15	18.65	38.66
lung	RL5	0.49	10.56		
	RS	1.10	19.66		
heart	RL5	0.39	19.01	33.09	56.00
	RS	0.22	23.40	65.40	102.00
kidney	RL5	2.34	63.53	29.30	39.70
	RS	2.82	132.25	26.25	45.07

3.8. *In Vivo* Pharmacokinetic and Tissue Distribution. Liposome drug delivery systems (DDS) are excellent candidates to circumvent the limitations of free RS. An assessment of pharmacokinetic profile of RL5 in comparison with that of free RS was performed by using standard protocols. Results of the pharmacokinetic evaluation of RL5 after intraperitoneal injection in Wistar rats are shown in Table 5. The higher concentration of RS from RL5 in the plasma and liver was achieved when compared to the animal group, which received free RS. The increase in the plasma concentration of RS in animals treated with RL5 could be due to opsonization and macrophage uptake of liposomes.[30] Furthermore, the positive charge on liposome slows down the absorption rate due to the electrostatic interaction between the positively charged liposomes and the negatively charged peritoneal mesothelium surface. The slow absorption is further prolonged due to the low uptake of positive liposomes by peritoneal macrophages.[74] Vesicle size is known as one of the critical parameters that impact the absorption, retention, and lymphatic uptake of liposomes following intraperitoneal injection.[75] Hirano and Hunt et al. explained that the stability of liposomes is important for the delivery of intact liposomes after intraperitoneal injection. Poor stability of large liposomes leads to fusion of liposomes and subsequent undesirable leakage of payload in the peritoneal cavity.[76] Lee et al. and Dadashzadeh et al. also suggested that there is a possibility of aggregation of cationic liposomes after intraperitoneal injection due to an increase in vesicle size. Hence, size is considered as an important factor for the efficient delivery of liposomes through intraperitoneal injection.[75,77] In terms of distribution, cationic liposomes were concentrated maximum in the liver, followed by the spleen (C_{max} 2.83 μg/mL, half-life of 30 min) as compared to other organs. This difference in the distribution could be attributed to the EPR effect and/or electrostatic interaction, as explained in Figure 1.[65,67] Electrostatic interaction between the positively charged liposomes and negatively charged hepatocellular cancer cells makes the drug delivery system a potential way of targeting anti-cancer drugs to liver cancer. In a healthy condition, the liver comprises PS, which is positioned internally (unexposed) in healthy liver tissue and is mediated by a membrane protein or ATP-dependent transporter, amino phospholipid translocase.[78,79] This symmetry of PS phospholipid is lost in cancer tissues because of decreased functional activity of enzyme-translocase and/or oxidative stress in the tumor microenvironment or activation of the scramblase enzyme. The loss of symmetry thus exposes the PS on the surface of cancer tissue, which is a salient feature of cancerous cells specifically endothelial cells (ECs).[31,80] The exposure of PS on the surface of cells, known as the death knell, generates a negative charge on liver cancer tissue.[67,81] Pharmacokinetic evaluation, therefore, serves as clear indicative of this mechanism, explaining the use of cationic liposomes as a potential targeting approach to the hepatocellular carcinoma.[82−84]

3.9. Anti-Cancer Efficiency of RS and RL5 in the Experimentally Induced Animal Model. Prophylactic and therapeutic anti-cancer properties of RL5 were assessed in NDEA induced HCC rats. The morphologies of liver, histopathology, relative body/liver weight ratio, tumor nodules, and liver enzyme levels (alanine transaminase (ALT), alkaline phosphatase (ALP), aspartate transaminase (AST), total bilirubin levels, γ-glutamyl transpeptidase (GGT) and α-fetoprotein (AFP)) were assessed in all groups to compare the efficiency of RL5 with free RS. At the end of ninth week of the experiment, two rats from the disease control group were dissected and liver samples were examined through histopathology to confirm successful induction of cancer in the liver. The morphology of liver specimens was analyzed after 12 weeks of the experimental period for all the groups (Figure 6 IA−F). The administration of RS and RL5 to HCC-bearing rats (Groups III−VI) showed very few hepatic nodules (Figure 6IIIB), as compared to the disease control group. The preventive and therapeutic RL5 treated rats (Groups IV and VI) showed a marked suppression in tumor development with significant changes in liver morphology, as compared to the disease control group.

Histological examination revealed that administration of NDEA induced granular cytoplasm with a condensed nucleus with the presence of Councilman bodies, mononuclear inflammatory cells, Kupffer cell hyperplasia, and neoplastic lesion (Figure 6 IIB−E). In both prophylactic and therapeutic treatment groups, the administration of RS and RL5 showed that RL5 was better than free RS in the prevention of damage and reduced the number of neoplastic lesions (Figure 6IIF−I). RS is known to prevent the progression of cancer by targeting multiple cellular targets affecting the cellular proliferation and growth: apoptosis, inflammation, invasion, angiogenesis, and metastasis. Bishayee et al. demonstrated that RS inhibits hepatic carcinogen-activating enzymes such as cytochrome P450 1A1(CYP1A1) and CYP3A/2 *in vitro* and *in vivo*.[85] Similar observations were reported by Dhir et al. and Rajasekaran et al. which showed that RS significantly decrease the number of nodules and progression of cancer in NDEA induced HCC in rodents.[86,87] NDEA administration to rats

https://dx.doi.org/10.1021/acsbiomaterials.0c00429
ACS Biomater. Sci. Eng. XXXX, XXX, XXX−XXX

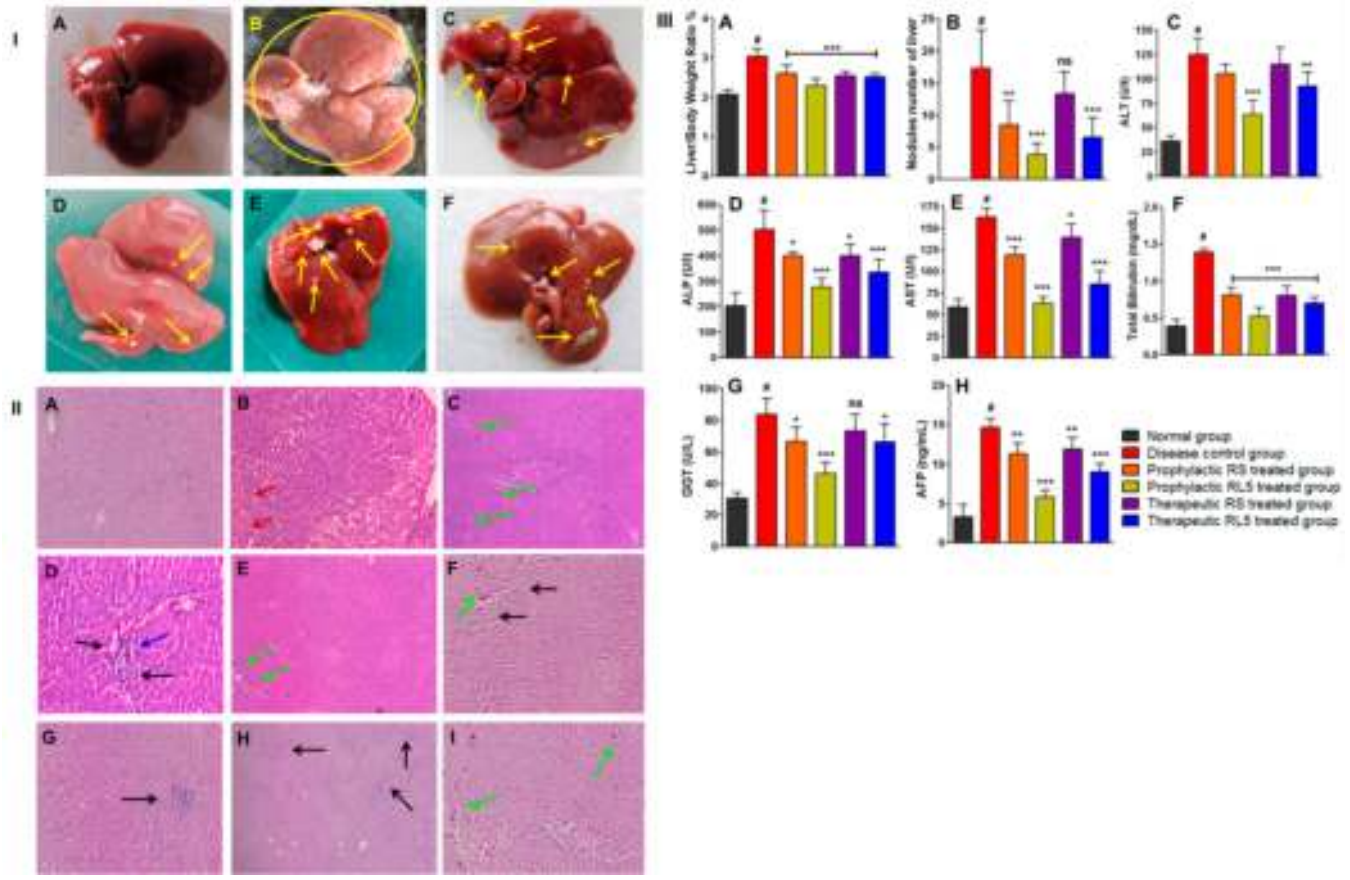

Figure 6. (I) Representative images of rat's livers: (A) normal group liver tissue appears normal with no macroscopically detectable pathological changes. (B) Disease control group liver tissues demonstrated significant changes in terms of color, consistency, and the surface texture. Tissue appeared pale pink in color with increased size and corrugated surface with multiple macroscopic nodules (yellow arrows). (C) Prophylactic RS treated group demonstrated very few nodules (yellow arrows) and lesions. (D) Prophylactic RL5 treated group in rats showed marked reduction in the number of nodules and damaged caused by NDEA. (E and F) Therapeutic RS and RL5 treated groups in rats showed reduction in the number of nodules. (II) Histopathological images of rat's livers: (A) Normal group showed normal hepatic lobule between the central vein and normal peripheral interlobular septum with the portal area comprising a portal vein, hepatic arteries bile ducts, and lymphatic vessels. (B–E) Disease control group showed injuries mainly as enlarged hepatocytes with granular cytoplasm with condensed nucleus (ballooning degeneration) with the presence of Councilman body (red arrows) and infiltration by mononuclear inflammatory cells (black arrows), kupffer cell hyperplasia (blue arrows), and neoplastic lesion, which is multicentric in origin (green arrows), was seen. (F) Prophylactic RS treated group showed neoplastic lesions with inflammatory cells, revealing the moderate improvement over the NDEA treated animals. (G) Prophylactic RL5 treated group showed hepatocyte maintaining normal architecture. (H) Therapeutic RS treated group showed neoplastic lesions. (I) Therapeutic RL5 treated group showed inflammatory cells in portal tract with moderate improvement over those of the disease control group. (III) (A) Liver/body weight ratio significant reduction in the liver/body weight ratio after administration of RS and RL5 as compared to disease control group. (B) Number of nodules on liver in each group; prophylactic and therapeutic RLs treated groups showed a significantly ($P < 0.001$) less number of nodules. (C–H) Enzyme estimations: the activities of serum alanine transaminase (ALT), alkaline phosphatase (ALP), aspartate transaminase (AST), total bilirubin levels, γ-glutamyl transpeptidase (GGT), and α-fetoprotein (AFP) were measured to assess the degree of hepatic cell damage. The data were shown as mean ± SD of six animals and statistically analyzed by one way ANOVA. Statistical significance was considered at $^{\#}P < 0.001$ when compared with the normal group; $^{***}P < 0.001$, $^{**}P < 0.01$, $^{*}P < 0.05$, and ns: no significance when compared with the disease control group.

lead to a marked elevation in levels of serum AST, ALT, ALP total bilirubin, and GGT levels, as shown in Figure 6IIIC–G, which is an indication of hepatocellular damage. Metabolism of NDEA in the liver causes damage to liver cells due to generation of reactive oxygen species (ROS). This process triggers uncontrolled proliferation of hepatocyte, ultimately leading to the generation of HCC.[88,89] RL5 treatment to HCC-bearing rats showed a significant decrease in the activities of AST, ALT, ALP, and GGT as compared to the disease control group.

Serum α fetoprotein (AFP) is considered as one of the key marker enzymes that is reported to increase in several diseases/disorders including hepatocellular carcinoma.[88] The effect of RS and RL5 on α-fetoprotein protein levels in NDEA induced liver damage is shown in Figure 6IIIH. Comparative AFP levels estimation of HCC induced rats treated with RS and RL5 clearly shows that RL5 treated rats had lower AFP levels than rats treated with free RS. Preventive and therapeutic treatment with RS and RL5 showed a significant decrease ($P < 0.001$) in AFP levels compared to those of disease control rats.

Overall, the cell uptake studies described above clearly support the idea that cationic liposomes have an inherent inclination toward PS groups present on the cancer cells, which was evident by higher internalization of RL5 than RS. These outcomes represent a novel strategy to target cancerous cells and can be used as an effective platform for the delivery of drugs and biological molecules for the treatment of HCC. The outcomes corroborate with the *in vivo* results discussed above,

https://dx.doi.org/10.1021/acsbiomaterials.0c00429
ACS Biomater. Sci. Eng. XXXX, XXX, XXX–XXX

which not only shows improvement in the therapeutic efficiency of the optimized RL5 compared to free RS but also confirms the biocompatible nature of the liposomes. Looking forward, it would be worth performing an experiment in combination with sorafenib (USFDA approved drug) to evaluate the effect of combination therapy.

4. CONCLUSION

In spite of its well-known application in cancer therapeutics, the use of RS is limited due to its physiological properties such as poor bioavailability and low half-life. Liposomes are one of the potential formulation systems approved by the FDA for application in cancer therapeutics. In the present investigation, we attempted to improve the bioavailability and the kinetic profile of RS by using cationic liposomes as a carrier for HCC. Optimized RL5 with a SL/Chol ratio of 7:2 and SA (5 mg) demonstrated desirable VS (145.78 ± 9.9 nm), ZP (38.03 ± 9.12 mV), and EE (78.14 ± 8.04%) values. The *in vitro* biocompatible nature of RLs was confirmed by the absence of cytotoxicity against fibroblast (L929) cell lines and blood erythrocytes. *In vitro* cell culture assay showed an enhanced uptake of RL5 in HepG2 cells, resulting in enhanced tumor cell killing ability when compared to free RS. This could be due to the high affinity of positively charged liposomes toward the negative charge of phosphatidylserine exposed on cancer cells. *In vivo* pharmacokinetic and pharmacodynamic studies revealed selective accumulation of RLs in liver cancer tissue, which demonstrated both chemopreventive and therapeutic effects on NDEA initiated HCC. Taken together, RS loaded cationic liposomes delivery system has a promising potential for the treatment of HCC and may provide a platform to enhance the delivery of small molecule anti-cancer drugs.

■ ASSOCIATED CONTENT

Supporting Information

The Supporting Information is available free of charge on the ACS Publications Web site. The Supporting Information is available free of charge at https://pubs.acs.org/doi/10.1021/acsbiomaterials.0c00429.

Table of results of analysis of variance test and figures of drug release kinetics models graphs, *in vitro* percentage hemolysis assay, and results of *in vivo* toxicity studies (PDF)

■ AUTHOR INFORMATION

Corresponding Authors

Satveer Jagwani − *KLE College of Pharmacy, Belagavi and Dr. Prabhakar Kore Basic Science Research Center, KLE Academy of Higher Education and Research, Belagavi 590010, Karnataka, India;* orcid.org/0000-0001-6754-174X; Phone: +91 8951002324; Email: satveerjagwani22@gmail.com

Sunil Jalalpure − *KLE College of Pharmacy, Belagavi and Dr. Prabhakar Kore Basic Science Research Center, KLE Academy of Higher Education and Research, Belagavi 590010, Karnataka, India;* orcid.org/0000-0001-7598-5973; Phone: +91 9448964057; Email: jalalpuresunil@rediffmail.com

Authors

Dinesh Dhamecha − *Dr. Prabhakar Kore Basic Science Research Center, KLE Academy of Higher Education and Research, Belagavi 590010, Karnataka, India*

Kiran Jadhav − *KLE College of Pharmacy, Belagavi, KLE Academy of Higher Education and Research, Belagavi 590010, Karnataka, India;* orcid.org/0000-0002-0502-1770

Raghvendra Bohara − *Centre for Interdisciplinary Research, D. Y. Patil Education Society (Institution Deemed to be University), Kolhapur 416006, Maharashtra, India; CÚRAM, SFI Research Centre for Medical Devices, National University of Ireland, Galway H91 W2TY, Ireland;* orcid.org/0000-0001-6654-9627

Complete contact information is available at: https://pubs.acs.org/10.1021/acsbiomaterials.0c00429

Author Contributions

⊥S.J. and D.D. contributed equally

Notes

The authors declare no competing financial interest.

■ ACKNOWLEDGMENTS

Authors would like to sincerely thank the KLE Academy of Higher Education and Research (formerly known as KLE University), Belagavi, Karnataka, India for providing financial support and the research facilities. The authors gratefully acknowledge Sami Labs, Bangalore, India for gifting pure trans-resveratrol and Lipoid GmbH, Ludwigshafen, Germany for providing (LIPOID S 100) phospholipid for the study. We would like to thank Dr. Ramesh Chavan, Department of Pathology, Jawaharlal Nehru Medical College, KAHER, Belagavi, for helping in the histopathology studies. The authors also would like to acknowledge SAIF, Indian Institute of Technology-Bombay, Mumbai, India for TEM analysis. Raghvendra Bohara would like to acknowledge the Irish Research Council, Ireland.

■ REFERENCES

(1) Bray, F.; Ferlay, J.; Soerjomataram, I.; Siegel, R. L.; Torre, L. A.; Jemal, A. Global Cancer Statistics 2018: GLOBOCAN Estimates of Incidence and Mortality Worldwide for 36 Cancers in 185 Countries. *Ca-Cancer J. Clin.* **2018**, *68* (6), 394−424.

(2) Llovet, J. M.; Villanueva, A.; Lachenmayer, A.; Finn, R. S. Advances in Targeted Therapies for Hepatocellular Carcinoma in the Genomic Era. *Nat. Rev. Clin. Oncol.* **2015**, *12*, 408−424.

(3) Okusaka, T.; Ikeda, M. Immunotherapy for Hepatocellular Carcinoma: Current Status and Future Perspectives. *ESMO open* **2018**, *3*, No. e000455.

(4) Chikara, S.; Nagaprashantha, L. D.; Singhal, J.; Horne, D.; Awasthi, S.; Singhal, S. S. Oxidative Stress and Dietary Phytochemicals: Role in Cancer Chemoprevention and Treatment. *Cancer Lett.* **2018**, *413*, 122−134.

(5) Bishayee, A. Cancer Prevention and Treatment with Resveratrol: From Rodent Studies to Clinical Trials. *Cancer Prev. Res.* **2009**, *2* (5), 409−418.

(6) Yin, S.; Xia, C.; Wang, Y.; Wan, D.; Rao, J.; Tang, X.; Wei, J.; Wang, X.; Li, M.; Zhang, Z.; Liu, J.; He, Q. Dual Receptor Recognizing Liposomes Containing Paclitaxel and Hydroxychloroquine for Primary and Metastatic Melanoma Treatment via Autophagy-Dependent and Independent Pathways. *J. Controlled Release* **2018**, *288*, 148−160.

(7) Teng, W.; Zhao, L.; Yang, S.; Zhang, C.; Liu, M.; Luo, J.; Jin, J.; Zhang, M.; Bao, C.; Li, D.; Xiong, W.; Li, Y.; Ren, F. The Hepatic-Targeted, Resveratrol Loaded Nanoparticles for Relief of High Fat

Diet-Induced Nonalcoholic Fatty Liver Disease. *J. Controlled Release* **2019**, *307*, 139−149.
(8) Öztürk, E.; Arslan, A. K. K.; Yerer, M. B.; Bishayee, A. Resveratrol and Diabetes: A Critical Review of Clinical Studies. *Biomed. Pharmacother.* **2017**, *95*, 230−234.
(9) Lu, Y.; Lu, X.; Wang, L.; Yang, W. Resveratrol Attenuates High Fat Diet-Induced Mouse Cardiomyopathy through Upregulation of Estrogen Related Receptor-α. *Eur. J. Pharmacol.* **2019**, *843*, 88−95.
(10) Cote, B.; Carlson, L. J.; Rao, D. A.; Alani, A. W. G. Combinatorial Resveratrol and Quercetin Polymeric Micelles Mitigate Doxorubicin Induced Cardiotoxicity in Vitro and in Vivo. *J. Controlled Release* **2015**, *213*, 128−133.
(11) Fernández-Quintela, A.; Milton-Laskibar, I.; González, M.; Portillo, M. P. Antiobesity Effects of Resveratrol: Which Tissues Are Involved? *Ann. N. Y. Acad. Sci.* **2017**, *1403* (1), 118−131.
(12) Sallem, F.; Haji, R.; Vervandier-Fasseur, D.; Nury, T.; Maurizi, L.; Boudon, J.; Lizard, G.; Millot, N. Elaboration of Trans-Resveratrol Derivative-Loaded Superparamagnetic Iron Oxide Nanoparticles for Glioma Treatment. *Nanomaterials* **2019**, *9* (2), 287.
(13) Jagwani, S.; Jalalpure, S.; Dhamecha, D.; Hua, G. S.; Jadhav, K. A Stability Indicating Reversed Phase HPLC Method for Estimation of Trans -Resveratrol in Oral Capsules and Nanoliposomes. *Anal. Chem. Lett.* **2019**, *9* (5), 711−726.
(14) Devulapally, R.; Foygel, K.; Sekar, T. V.; Willmann, J. K.; Paulmurugan, R. Gemcitabine and Antisense-MicroRNA Co-Encapsulated PLGA-PEG Polymer Nanoparticles for Hepatocellular Carcinoma Therapy. *ACS Appl. Mater. Interfaces* **2016**, *8* (49), 33412−33422.
(15) Chishti, N.; Jagwani, S.; Dhamecha, D.; Jalalpure, S.; Dehghan, M. H. Preparation, Optimization, and in Vivo Evaluation of Nanoparticle-Based Formulation for Pulmonary Delivery of Anticancer Drug. *Med.* **2019**, *55* (6), 294.
(16) Jadhav, K.; HR, R.; Deshpande, S.; Jagwani, S.; Dhamecha, D.; Jalalpure, S.; Subburayan, K.; Baheti, D. Phytosynthesis of Gold Nanoparticles: Characterization, Biocompatibility, and Evaluation of Its Osteoinductive Potential for Application in Implant Dentistry. *Mater. Sci. Eng., C* **2018**, *93*, 664−670.
(17) Dhamecha, D.; Jalalpure, S.; Jadhav, K. Doxorubicin Functionalized Gold Nanoparticles: Characterization and Activity against Human Cancer Cell Lines. *Process Biochem.* **2015**, *50* (12), 2298−2306.
(18) Jadhav, K.; Dhamecha, D.; Bhattacharya, D.; Patil, M. Green and Ecofriendly Synthesis of Silver Nanoparticles: Characterization, Biocompatibility Studies and Gel Formulation for Treatment of Infections in Burns. *J. Photochem. Photobiol., B* **2016**, *155*, 109−115.
(19) Tang, M.; Svirskis, D.; Leung, E.; Kanamala, M.; Wang, H.; Wu, Z. Can Intracellular Drug Delivery Using Hyaluronic Acid Functionalised PH-Sensitive Liposomes Overcome Gemcitabine Resistance in Pancreatic Cancer? *J. Controlled Release* **2019**, *305*, 89−100.
(20) H.R., R.; Dhamecha, D.; Jagwani, S.; Rao, M.; Jadhav, K.; Shaikh, S.; Puzhankara, L.; Jalalpure, S. Local Drug Delivery Systems in the Management of Periodontitis: A Scientific Review. *J. Controlled Release* **2019**, *307*, 393−409.
(21) Zhang, N.; Chen, H.; Liu, A. Y.; Shen, J. J.; Shah, V.; Zhang, C.; Hong, J.; Ding, Y. Gold Conjugate-Based Liposomes with Hybrid Cluster Bomb Structure for Liver Cancer Therapy. *Biomaterials* **2016**, *74*, 280−291.
(22) Kushwah, V.; Jain, D. K.; Agrawal, A. K.; Jain, S. Improved Antitumor Efficacy and Reduced Toxicity of Docetaxel Using Anacardic Acid Functionalized Stealth Liposomes. *Colloids Surf., B* **2018**, *172*, 213−223.
(23) Wang, M.; Liu, Y.; Zhang, X.; Luo, L.; Li, L.; Xing, S.; He, Y.; Cao, W.; Zhu, R.; Gao, D. Gold Nanoshell Coated Thermo-PH Dual Responsive Liposomes for Resveratrol Delivery and Chemo-Photothermal Synergistic Cancer Therapy. *J. Mater. Chem. B* **2017**, *5* (11), 2161−2171.
(24) Cosco, D.; Paolino, D.; Maiuolo, J.; Marzio, L. Di; Carafa, M.; Ventura, C. A.; Fresta, M. Ultradeformable Liposomes as Multidrug Carrier of Resveratrol and 5-Fluorouracil for Their Topical Delivery. *Int. J. Pharm.* **2015**, *489* (1−2), 1−10.
(25) Caddeo, C.; Teskač, K.; Sinico, C.; Kristl, J. Effect of Resveratrol Incorporated in Liposomes on Proliferation and UV-B Protection of Cells. *Int. J. Pharm.* **2008**, *363* (1−2), 183−191.
(26) Caddeo, C.; Nacher, A.; Vassallo, A.; Armentano, M. F.; Pons, R.; Fernàndez-Busquets, X.; Carbone, C.; Valenti, D.; Fadda, A. M.; Manconi, M. Effect of Quercetin and Resveratrol Co-Incorporated in Liposomes against Inflammatory/Oxidative Response Associated with Skin Cancer. *Int. J. Pharm.* **2016**, *513* (1−2), 153−163.
(27) Jhaveri, A.; Deshpande, P.; Pattni, B.; Torchilin, V. Transferrin-Targeted, Resveratrol-Loaded Liposomes for the Treatment of Glioblastoma. *J. Controlled Release* **2018**, *277*, 89−101.
(28) Pozo-Guisado, E.; Merino, J. M.; Mulero-Navarro, S.; Lorenzo-Benayas, M. J.; Centeno, F.; Alvarez-Barrientos, A.; Salguero, P. M. F. Resveratrol-Induced Apoptosis in MCF-7 Human Breast Cancer Cells Involves a Caspase-Independent Mechanism with Downregulation of Bcl-2 and NF-KB. *Int. J. Cancer* **2005**, *115* (1), 74−84.
(29) Narayanan, N. K.; Nargi, D.; Randolph, C.; Narayanan, B. A. Liposome Encapsulation of Curcumin and Resveratrol in Combination Reduces Prostate Cancer Incidence in PTEN Knockout Mice. *Int. J. Cancer* **2009**, *125* (1), 1−8.
(30) Bilensoy, E. Cationic Nanoparticles for Cancer Therapy. *Expert Opin. Drug Delivery* **2010**, *7* (7), 795−809.
(31) Fidler, I. J.; Schroit, A. J.; Connor, J.; Bucana, C. D.; Fidler, I. J. Elevated Expression of Phosphatidylserine in the Outer Membrane Leaflet of Human Tumor Cells and Recognition by Activated Human Blood Monocytes. *Cancer Res.* **1991**, *51* (11), 3062−3066.
(32) Bangham, A. D.; Standish, M. M.; Watkins, J. C. Diffusion of Univalent Ions across the Lamellae of Swollen Phospholipids. *J. Mol. Biol.* **1965**, *13* (1), 238−252.
(33) Jain, S.; Kumar, D.; Swarnakar, N. K.; Thanki, K. Biomaterials Polyelectrolyte Stabilized Multilayered Liposomes for Oral Delivery of Paclitaxel Q. *Biomaterials* **2012**, *33* (28), 6758−6768.
(34) Liu, J.; Wang, Z.; Li, F.; Gao, J.; Wang, L.; Huang, G. Liposomes for Systematic Delivery of Vancomycin Hydrochloride to Decrease Nephrotoxicity: Characterization and Evaluation. *Asian J. Pharm. Sci.* **2015**, *10* (3), 212−222.
(35) Nguyen, T. L.; Nguyen, T. H.; Nguyen, D. H. Development and in Vitro Evaluation of Liposomes Using Soy Lecithin to Encapsulate Paclitaxel. *Int. J. Biomater.* **2017**, *2017*, 1.
(36) Shishir, M. R. I.; Karim, N.; Gowd, V.; Xie, J.; Zheng, X.; Chen, W. Pectin-Chitosan Conjugated Nanoliposome as a Promising Delivery System for Neohesperidin: Characterization, Release Behavior, Cellular Uptake, and Antioxidant Property. *Food Hydrocolloids* **2019**, *95*, 432−444.
(37) Shah, S. M.; Goel, P. N.; Jain, A. S.; Pathak, P. O.; Padhye, S. G.; Govindarajan, S.; Ghosh, S. S.; Chaudhari, P. R.; Gude, R. P.; Gopal, V.; Nagarsenker, M. S. Liposomes for Targeting Hepatocellular Carcinoma: Use of Conjugated Arabinogalactan as Targeting Ligand. *Int. J. Pharm.* **2014**, *477* (1−2), 128−139.
(38) Karn, P. R.; Cho, W.; Park, H. J.; Park, J. S.; Hwang, S. J. Characterization and Stability Studies of a Novel Liposomal Cyclosporin a Prepared Using the Supercritical Fluid Method: Comparison with the Modified Conventional Bangham Method. *Int. J. Nanomed.* **2013**, *8*, 365−377.
(39) Jadhav, K.; Deore, S.; Dhamecha, D.; Hr, R.; Jagwani, S.; Jalalpure, S.; Bohara, R. Phytosynthesis of Silver Nanoparticles: Characterization, Biocompatibility Studies, and Anticancer Activity. *ACS Biomater. Sci. Eng.* **2018**, *4* (3), 892−899.
(40) Dhamecha, D.; Jalalpure, S.; Jadhav, K.; Jagwani, S.; Chavan, R. Doxorubicin Loaded Gold Nanoparticles: Implication of Passive Targeting on Anticancer Efficacy. *Pharmacol. Res.* **2016**, *113*, 547−556.
(41) Rajeshwari, H. R.; Dhamecha, D.; Jagwani, S.; Patil, D.; Hegde, S.; Potdar, R.; Metgud, R.; Jalalpure, S.; Roy, S.; Jadhav, K.; Tiwari, N. K.; Koduru, S.; Hugar, S.; Dodamani, S. Formulation of Thermoreversible Gel of Cranberry Juice Concentrate: Evaluation,

https://dx.doi.org/10.1021/acsbiomaterials.0c00429
ACS Biomater. Sci. Eng. XXXX, XXX, XXX−XXX

Biocompatibility Studies and Its Antimicrobial Activity against Periodontal Pathogens. *Mater. Sci. Eng., C* **2017**, *75*, 1506−1514.
(42) Garg, N. K.; Singh, B.; Kushwah, V.; Tyagi, R. K.; Sharma, R.; Jain, S.; Katare, O. P. The Ligand (s) Anchored Lipobrid Nanoconstruct Mediated Delivery of Methotrexate: An Effective Approach in Breast Cancer Therapeutics. *Nanomedicine* **2016**, *12* (7), 2043−2060.
(43) Pretor, S.; Bartels, J.; Lorenz, T.; Dahl, K.; Finke, J. H.; Peterat, G.; Krull, R.; Al-Halhouli, A. T.; Dietzel, A.; Büttgenbach, S.; Behrends, S.; Reichl, S.; Müller-Goymann, C. C. Cellular Uptake of Coumarin-6 under Microfluidic Conditions into HCE-T Cells from Nanoscale Formulations. *Mol. Pharmaceutics* **2015**, *12* (1), 34−45.
(44) Kilkenny, C.; Browne, W. J.; Cuthill, I. C.; Emerson, M.; Altman, D. G. The ARRIVE Guidelines Animal Research: Reporting in Vivo Experiments. *PLoS Biol.* **2010**, *8* (6), No. e1000412.
(45) El Mesallamy, H. O.; Metwally, N. S.; Soliman, M. S.; Ahmed, K. A.; Moaty, M. M. A. The Chemopreventive Effect of Ginkgo Biloba and Silybum Marianum Extracts on Hepatocarcinogenesis in Rats. *Cancer Cell Int.* **2011**, *11* (1), 38.
(46) Lee, E. O.; Lee, H. J.; Hwang, H. S.; Ahn, K. S.; Chae, C.; Kang, K. S.; Lu, J.; Kim, S. H. Potent Inhibition of Lewis Lung Cancer Growth by Heyneanol A from the Roots of Vitis Amurensis through Apoptotic and Anti-Angiogenic Activities. *Carcinogenesis* **2006**, *27* (10), 2059−2069.
(47) Diehl, K. H.; Hull, R.; Morton, D.; Pfister, R.; Rabemampianina, Y.; Smith, D.; Vidal, J. M.; Van De Vorstenbosch, C. A Good Practice Guide to the Administration of Substances and Removal of Blood, Including Routes and Volumes. *J. Appl. Toxicol.* **2001**, *21* (1), 15−23.
(48) Jagwani, S.; Jalalpure, S.; Dhamecha, D.; Hua, G. S.; Jadhav, K. Development and Validation of Reverse-Phase High-Performance Liquid Chromatographic Method for Determination of Resveratrol in Human and Rat Plasma for Preclinical and Clinical Studies. *Indian J. Pharm. Educ.* **2019**, *54* (1), 187−193.
(49) Tsai, Y. M.; Chien, C. F.; Lin, L. C.; Tsai, T. H. Curcumin and Its Nano-Formulation: The Kinetics of Tissue Distribution and Blood-Brain Barrier Penetration. *Int. J. Pharm.* **2011**, *416* (1), 331−338.
(50) Shelke, S.; Shahi, S.; Jalalpure, S.; Dhamecha, D. Poloxamer 407-Based Intranasal Thermoreversible Gel of Zolmitriptan-Loaded Nanoethosomes: Formulation, Optimization, Evaluation and Permeation Studies. *J. Liposome Res.* **2016**, *26* (4), 313−323.
(51) Kotyńska, J.; Figaszewski, Z. A. Adsorption Equilibria at Interface Separating Electrolyte Solution and Phosphatidylcholine−Stearylamine Liposome Membrane. *Biophys. Chem.* **2007**, *127* (1−2), 84−90.
(52) Villasmil-Sánchez, S.; Drhimeur, W.; Ospino, S. C. S.; Rabasco Alvarez, A. M.; González-Rodríguez, M. L. Positively and Negatively Charged Liposomes as Carriers for Transdermal Delivery of Sumatriptan: In Vitro Characterization. *Drug Dev. Ind. Pharm.* **2010**, *36* (6), 666−675.
(53) Ramana, L. N.; Sethuraman, S.; Ranga, U.; Krishnan, U. M. Development of a Liposomal Nanodelivery System for Nevirapine. *J. Biomed. Sci.* **2010**, *17* (1), 57.
(54) El Maghraby, G. M. M.; Campbell, M.; Finnin, B. C. Mechanisms of Action of Novel Skin Penetration Enhancers: Phospholipid versus Skin Lipid Liposomes. *Int. J. Pharm.* **2005**, *305* (1−2), 90−104.
(55) Dhamecha, D.; Jalalpure, S.; Jadhav, K. Nepenthes Khasiana Mediated Synthesis of Stabilized Gold Nanoparticles: Characterization and Biocompatibility Studies. *J. Photochem. Photobiol., B* **2016**, *154*, 108−117.
(56) Casals, E.; Soler, M.; Gallardo, M.; Estelrich, J. Electrophoretic Behavior of Stearylamine-Containing Liposomes. *Langmuir* **1998**, *14* (26), 7522−7526.
(57) González-Rodríguez, M. L.; Rabasco, A. M. Charged Liposomes as Carriers to Enhance the Permeation through the Skin. *Expert Opin. Drug Delivery* **2011**, *8* (7), 857−871.
(58) Hammoud, Z.; Gharib, R.; Fourmentin, S.; Elaissari, A.; Greige-Gerges, H. Drug-in-Hydroxypropyl-β-Cyclodextrin-in-Lipoid S100/Cholesterol Liposomes: Effect of the Characteristics of Essential Oil Components on Their Encapsulation and Release. *Int. J. Pharm.* **2020**, *579*, 119151.
(59) Karve, S.; Kempegowda, G. B.; Sofou, S. Heterogeneous Domains and Membrane Permeability in Phosphatidylcholine - Phosphatidic Acid Rigid Vesicles as a Function of PH and Lipid Chain Mismatch. *Langmuir* **2008**, *24* (11), 5679−5688.
(60) Bruschi, M. L. Mathematical Models of Drug Release. *Strategies to Modify the Drug Release from Pharmaceutical Systems*; Woodhead Publishing, 2015. .
(61) Wójcik-Pastuszka, D.; Krzak, J.; Macikowski, B.; Berkowski, R.; Osiński, B.; Musiał, W. Evaluation of the Release Kinetics of a Pharmacologically Active Substance from Model Intra-Articular Implants Replacing the Cruciate Ligaments of the Knee. *Materials* **2019**, *12* (8), 1202.
(62) Dhawan, V.; Magarkar, A.; Joshi, G.; Makhija, D.; Jain, A.; Shah, J.; Reddy, B. V. V.; Krishnapriya, M.; Róg, T.; Bunker, A.; Jagtap, A.; Nagarsenker, M. Stearylated Cycloarginine Nanosystems for Intracellular Delivery-Simulations, Formulation and Proof of Concept. *RSC Adv.* **2016**, *6* (114), 113538−113550.
(63) Su, D.; Cheng, Y.; Liu, M.; Liu, D.; Cui, H.; Zhang, B.; Zhou, S.; Yang, T.; Mei, Q. Comparision of Piceid and Resveratrol in Antioxidation and Antiproliferation Activities In Vitro. *PLoS One* **2013**, *8* (1), No. e54505.
(64) Lu, X.-Y.; Hu, S.; Jin, Y.; Qiu, L.-Y. Application of Liposome Encapsulation Technique to Improve Anti-Carcinoma Effect of Resveratrol. *Drug Dev. Ind. Pharm.* **2012**, *38* (3), 314−322.
(65) Wang, H.; Thorling, C. A.; Liang, X.; Bridle, K. R.; Grice, J. E.; Zhu, Y.; Crawford, D. H. G.; Xu, Z. P.; Liu, X.; Roberts, M. S. Diagnostic Imaging and Therapeutic Application of Nanoparticles Targeting the Liver. *J. Mater. Chem. B* **2015**, *3* (6), 939−958.
(66) Kristl, J.; Teskač, K.; Caddeo, C.; Abramović, Z.; Šentjurc, M. Improvements of Cellular Stress Response on Resveratrol in Liposomes. *Eur. J. Pharm. Biopharm.* **2009**, *73* (2), 253−259.
(67) De, M.; Ghosh, S.; Sen, T.; Shadab, M.; Banerjee, I.; Basu, S.; Ali, N. A Novel Therapeutic Strategy for Cancer Using Phosphatidylserine Targeting Stearylamine-Bearing Cationic Liposomes. *Mol. Ther.–Nucleic Acids* **2018**, *10*, 9−27.
(68) Miao, X.; Li, Y.; Wyman, I.; Lee, S. M. Y.; Macartney, D. H.; Zheng, Y.; Wang, R. Enhanced in Vitro and in Vivo Uptake of a Hydrophobic Model Drug Coumarin-6 in the Presence of Cucurbit [7] Uril. *MedChemComm* **2015**, *6* (7), 1370−1374.
(69) Parvathaneni, V.; Kulkarni, N. S.; Shukla, S. K.; Farrales, P. T.; Kunda, N. K.; Muth, A.; Gupta, V. Systematic Development and Optimization of Inhalable Pirfenidone Liposomes for Non-Small Cell Lung Cancer Treatment. *Pharmaceutics* **2020**, *12* (3), 206.
(70) Rivolta, I.; Panariti, A.; Lettiero, B.; Sesana, S.; Gasco, P.; Gasco, M. R.; Masserini, M.; Miserocchi, G. Cellular Uptake of Coumarin-6 as a Model Drug Loaded in Solid Lipid Nanoparticles. *J. Physiol. Pharmacol.* **2011**, *62* (1), 45−53.
(71) Zhao, S.; Dai, W.; He, B.; Wang, J.; He, Z.; Zhang, X.; Zhang, Q. Monitoring the Transport of Polymeric Micelles across MDCK Cell Monolayer and Exploring Related Mechanisms. *J. Controlled Release* **2012**, *158* (3), 413−423.
(72) Saadat, M.; Zahednezhad, F.; Zakeri-Milani, P.; Heidari, H. R.; Shahbazi-Mojarrad, J.; Valizadeh, H. Drug Targeting Strategies Based on Charge Dependent Uptake of Nanoparticles into Cancer Cells. *J. Pharm. Pharm. Sci.* **2019**, *22*, 191−220.
(73) Behzadi, S.; Serpooshan, V.; Tao, W.; Hamaly, M. A.; Alkawareek, M. Y.; Dreaden, E. C.; Brown, D.; Alkilany, A. M.; Farokhzad, O. C.; Mahmoudi, M. Cellular Uptake of Nanoparticles: Journey inside the Cell. *Chem. Soc. Rev.* **2017**, *46* (14), 4218−4244.
(74) De Smet, L.; Ceelen, W.; Remon, J. P.; Vervaet, C. Optimization of Drug Delivery Systems for Intraperitoneal Therapy to Extend the Residence Time of the Chemotherapeutic Agent. *Sci. World J.* **2013**, *2013*, 1.

https://dx.doi.org/10.1021/acsbiomaterials.0c00429
ACS Biomater. Sci. Eng. XXXX, XXX, XXX−XXX

(75) Lee, G.; Han, S.; Inocencio, I.; Cao, E.; Hong, J.; Phillips, A. R. J.; Windsor, J. A.; Porter, C. J. H.; Trevaskis, N. L. Lymphatic Uptake of Liposomes after Intraperitoneal Administration Primarily Occurs via the Diaphragmatic Lymphatics and Is Dependent on Liposome Surface Properties. *Mol. Pharmaceutics* **2019**, *16* (12), 4987−4999.
(76) Hirano, K.; Hunt, C. A. Lymphatic Transport of Liposome-encapsulated Agents: Effects of Liposome Size Following Intraperitoneal Administration. *J. Pharm. Sci.* **1985**, *74* (9), 915−921.
(77) Dadashzadeh, S.; Mirahmadi, N.; Babaei, M. H.; Vali, a M. Peritoneal Retention of Liposomes: Effects of Lipid Composition, PEG Coating and Liposome Charge. *J. Controlled Release* **2010**, *148* (2), 177−186.
(78) Kenis, H.; Reutelingsperger, C. Targeting Phosphatidylserine in Anti-Cancer Therapy. *Curr. Pharm. Des.* **2009**, *15* (23), 2719−2723.
(79) Soares, M. M.; King, S. W.; Thorpe, P. E. Targeting Inside-out Phosphatidylserine as a Therapeutic Strategy for Viral Diseases. *Nat. Med.* **2008**, *14* (12), 1357−1362.
(80) Riedl, S.; Rinner, B.; Asslaber, M.; Schaider, H.; Walzer, S.; Novak, A.; Lohner, K.; Zweytick, D. In Search of a Novel Target - Phosphatidylserine Exposed by Non-Apoptotic Tumor Cells and Metastases of Malignancies with Poor Treatment Efficacy. *Biochim. Biophys. Acta, Biomembr.* **2011**, *1808* (11), 2638−2645.
(81) Ran, S.; Downes, A.; Thorpe, P. E. Increased Exposure of Anionic Phospholipids on the Surface of Tumor Blood Vessels. *Cancer Res.* **2002**, *62* (21), 6132−6140.
(82) Bozzuto, G.; Molinari, A. Liposomes as Nanomedical Devices. *Int. J. Nanomed.* **2015**, *10*, 975−999.
(83) Reddy, L. H.; Couvreur, P. Nanotechnology for Therapy and Imaging of Liver Diseases. *J. Hepatol.* **2011**, *55* (6), 1461−1466.
(84) Zhu, X.; Tsend-Ayush, A.; Yuan, Z.; Wen, J.; Cai, J.; Luo, S.; Yao, J.; Bian, J.; Yin, L.; Zhou, J.; Yao, J. Glycyrrhetinic Acid-Modified TPGS Polymeric Micelles for Hepatocellular Carcinoma-Targeted Therapy. *Int. J. Pharm.* **2017**, *529* (1−2), 451−464.
(85) Bishayee, A.; Politis, T.; Darvesh, A. S. Resveratrol in the Chemoprevention and Treatment of Hepatocellular Carcinoma. *Cancer Treat. Rev.* **2010**, *36* (1), 43−53.
(86) Bishayee, A.; Dhir, N. Resveratrol-Mediated Chemoprevention of Diethylnitrosamine-Initiated Hepatocarcinogenesis: Inhibition of Cell Proliferation and Induction of Apoptosis. *Chem.-Biol. Interact.* **2009**, *179* (2−3), 131−144.
(87) Rajasekaran, D.; Elavarasan, J.; Sivalingam, M.; Ganapathy, E.; Kumar, A.; Kalpana, K.; Sakthisekaran, D. Resveratrol Interferes with N-Nitrosodiethylamine-Induced Hepatocellular Carcinoma at Early and Advanced Stages in Male Wistar Rats. *Mol. Med. Rep.* **2011**, *4* (6), 1211−1217.
(88) Rajesh, V.; Kavitha, K. N. V. K.; Vishali, K.; Raju, C.; Gayathri, K.; Sruthi, A. Protective Effect Courouptia Guianensis Flower Extract against N-Nitrosodiethylamine-Induced Hepatic Damage in Wistar Albino Rats. *Orient. Pharm. Exp. Med.* **2015**, *15* (1), 83−93.
(89) Farazuddin, M.; Bhavyata, D.; Zia, Q.; Khan, A. A.; Joshi, B.; Owais, M. Chemotherapeutic Potential of Curcumin-Bearing Microcells against Hepatocellular Carcinoma in Model Animals. *Int. J. Nanomed.* **2014**, *9*, 1139.

https://dx.doi.org/10.1021/acsbiomaterials.0c00429
ACS Biomater. Sci. Eng. XXXX, XXX, XXX−XXX

Journal of Photochemistry & Photobiology, B: Biology 154 (2016) 108–117

Contents lists available at ScienceDirect

Journal of Photochemistry & Photobiology, B: Biology

journal homepage: www.elsevier.com/locate/jphotobiol

Nepenthes khasiana mediated synthesis of stabilized gold nanoparticles: Characterization and biocompatibility studies

Dinesh Dhamecha [a,b], Sunil Jalalpure [a,b,*], Kiran Jadhav [a]

[a] KLE University's College of Pharmacy, Nehru Nagar, Belgaum-590010, Karnataka, India
[b] Dr. Prabhakar Kore Basic Science Research Center, KLE University, Belgaum-590010, Karnataka, India

ARTICLE INFO

Article history:
Received 21 October 2015
Received in revised form 30 November 2015
Accepted 8 December 2015
Available online 9 December 2015

Keywords:
Antioxidant assay
Biocompatibility
Gold nanoparticles
Green chemistry
Nepenthes khasiana

ABSTRACT

The current study summarizes a unique green process for the synthesis of gold nanoparticles by simple treatment of gold salts with aqueous extract of *Nepenthes khasiana* (NK)—a red listed medicinal plant and its characterization. Study on the effect of different process parameters like temperature, pH and stirring on surface and stability characteristics has been demonstrated. Formation of GNPs was visually observed by change in color from colorless to wine red and characterized by UV-Visible spectroscopy, FT-IR spectroscopy, Zetasizer, X-RD, ICP-AES, SEM-EDAX, AFM and TEM. *In vitro* stability studies of gold colloidal dispersion in various blood components suggest that, NK mediated GNPs exhibit remarkable *in vitro* stability in 2% bovine serum albumin, 2% human serum albumin (HSA), 0.2 M histidine, and 0.2 M cysteine but unstable in 5% NaCl solution and acidic pH. Biocompatibility of NK stabilized GNPs against normal mouse fibroblasts (L929) cell lines revealed nontoxic nature of GNPs and thus provides exceptional opportunities for their uses as nanomedicine for diagnosis and drug therapy. The role of antioxidant phytochemicals (flavonoids and polyphenols) of NK extract in synthesis of biocompatible and stabilized GNPs was demonstrated by estimating total flavonoid content, total phenolic content and total antioxidant capacity of extract before and after formation of GNPs. Fast and easy synthesis of biocompatible GNPs possesses unique physical and chemical features which serve as an advantage for its use in various biomedical applications. The overall approach designated in the present research investigation for the synthesis of GNPs is based on all 12 principles of green chemistry, in which no man-made chemical other than the gold chloride was used.

1. Introduction

Nanobiotechnology is the growing interdisciplinary field of research connecting biological science, material science and nanotechnology. Gold nanoparticles (GNPs) owning to its unique surface plasmon resonance effect can be used in various biomedical applications like tumor targeting, tumor imaging, diagnosis, photonics, photothermal therapy and in electronic applications [1,2]. One of the main advantages of GNPs is their surface plasmon resonance effect, which aids for greater photon capture than those of photo thermal dyes [3] and nano size helps in cancer targeting and diagnosis. This bio-detection sensitivity of GNPs is often associated with their physical and chemical properties depending on the shape [4].

Even though different methods such as UV-irradiation, lithography, aerosol technology, and laser metal have been used to produce GNPs, they remain harmful and expensive. Hazardous materials such as hydroxylamine, sodium borohydride and tetra kis (hydroxylmethyl) phosphonium chloride [5–10] used in reduction and stabilization were found to cause adverse effect in biomedical applications [11–13]. Different methods described by Turkevic, Brust, and Perrault have demonstrated use of synthetic reducing agents for the preparation of GNPs, but most of these methods are extremely expensive and also involve the use of toxic, hazardous chemicals, which may pose potential biological and environmental risks as they generate a large amount of hazardous byproducts [7,14,15]. Hence, there is increasing need to develop high yielding, cost effective, nontoxic and environmental friendly process for preparation of GNPs. Thus, 'Green Chemistry' that uses plant extracts could be an alternative to synthetic method for the production of GNPs.

Extracellular and intracellular biological synthesis of metal nanoparticles by bacteria, fungi, actinomycetes, yeasts and plants is well reported. It reveals that extracellular synthesis of GNPs has more biomedical and commercial applications than intracellular synthesis. For example *Thermomonospora* sp., *Fusarium oxysporum* [16–18] synthesized extracellular GNPs whereas *Bacillus subtilis* and *Shewanella algae* [19–20] synthesized intracellular GNPs. But, successive purification of GNPs formed with microorganisms intracellularly is generally challenging [21] and selection of microbes for extracellular biosynthesis needs extensive screening [22] and vigorous cultivation of microorganisms. Although, use of microorganisms in the synthesis of GNPs is a

* Corresponding author at: Dr. Prabhakar Kore Basic Science Research Center, KLE University, Belgaum-590010, Karnataka, India.
E-mail addresses: dineshdhamecha@gmail.com (D. Dhamecha), jalalpuresunil@rediffmail.com (S. Jalalpure), kiranjadhavqa@gmail.com (K. Jadhav).

http://dx.doi.org/10.1016/j.jphotobiol.2015.12.002
1011-1344/

comparatively attractive area of research, use of plants extracts for synthesis of GNPs is more advantageous over microbial method by eliminating the elaborative process of preserving cell cultures, large scale synthesis, efficient recovery, simplicity (ease of synthesis) and ease of understanding the mechanism of synthesis.

Recently, only few plants like *Medicago sativa* [23] and *Sesbania drummondii* [24] have shown intracellular synthesis whereas plants like *Coleus amboinicus* [25], *Magnolia kobus* and *Diopyros kaki*, etc., [26] have shown extracellular synthesis of GNPs. Taking into consideration the variety of plants, the prospective use of plants as green source for synthesis of nanoparticles is yet to be fully explored.

Synthesis of GNPs with uniform size and shape is of foremost importance due to their prospective applications in medical devices, sensor technology, electronics, catalysis, optical devices and biological labeling [27–29]. It has been reported that optoelectric and physicochemical properties of GNPs are size and shape dependent [30–32]. Among heavy metals, research on GNPs received immense consideration due to its distinctive and tunable surface plasmon resonance [33].

GNPs have many applications in biomedical sciences including drug delivery, tissue/tumor imaging, photothermal applications and identification of pathogens in clinical specimens [34]. Use of plant extracts rich in antioxidants could be a particular interest to improve monodispersity of GNPs and to control their size and shape.

In the present study, leaves of *Nepenthes khasiana* (NK), a carnivorous plant species belonging to the family *Nepentheceae* were used for the synthesis of GNPs. NK popularly known as pitcher plant is recognized as one of the red listed plants by the International Union for the Conservation of Nature (IUCN) and is endemic to Meghalaya state of India [35]. Literature suggests that phytochemical like flavonoids and polyphenols represents the antioxidant potential of Nepenthes sp. and can be used as a green source for synthesis and stabilization of GNPs.

Till date, there are no reports regarding the phytochemical investigation of NK. Herein, the main objective of the research was to evaluate the presence of antioxidant principles of NK and to utilize its antioxidant potential for synthesis of GNPs. Finally, biocompatibility characteristics of NK mediated synthesized GNPs were evaluated against normal mouse fibroblasts cell lines (L929) using MTT assay.

2. Materials

N. khasiana leaves (NK) were collected from Shilong and authenticated from Botanical survey of India, Shilong, India. Gold (III) chloride hydrate (99.99% metal basis, used without further purification), cysteine, histidine, human serum albumin, and bovine serum albumin were procured from Sigma Aldrich, Bangalore, India. Dulbecco's modified Eagle medium (DMEM), fetal bovine serum (FBS), and Pen Strep (a mixture of penicillin and streptomycin) were procured from Gibco Life Technologies (Auckland, New Zealand); phosphomolybdate, quercetin, Folin Ciocalteu reagent, gentamycin (4 mg/ml) and amphotericin (5 mg/ml) were purchased from Himedia Pvt. Ltd., Mumbai, India. Mouse fibroblasts (L929 cell lines) were collected from the National Center for Cell Science, Pune, India.

3. Experimental

3.1. Preparation and evaluation of plant extract

Plant extract was prepared by boiling 10 g of air dried powdered plant material with 100 ml of deionized water for 10 min and filtered through Whatman filter paper 41#. Phytochemical investigation of filtrate was carried out to confirm the presence of carbohydrates, proteins, flavonoids, tannins and polyphenols. *In vitro* quantitative assay methods like total flavonoid content (TFC), total antioxidant capacity (TAC) and total phenolic content (TPC) were used for quantitative estimation of antioxidant potential of plant extract. TAC of the plant extracts was determined by phosphomolybdate method where quercetin was used as a standard, TPC was determined by using Folin Ciocalteu reagent where gallic acid was used as a standard [36] and TFC was performed according to aluminum chloride colorimetric method described by Chang et al. with slight modifications using quercetin as a standard [37].

3.2. Synthesis of GNPs

GNPs were prepared by adding aqueous plant extract to aqueous gold chloride solution (0.5 mM) in volume ratios of 10:1, 10:2 and 10:3. The bioreduction of gold salt was monitored by sampling at regular interval using aliquots (0.1 ml) of the mixture and analyzing UV–Visible spectra after suitable dilutions. Formation of GNPs was observed by visual color change and confirmed by UV–Visible spectroscopy (Hitachi-Inkarp 2300 SICAN, Inkarp Instruments Pvt. Ltd., Japan). The mixture was then filtered to remove the unwanted insoluble biomass and finally purified by using high speed refrigerated centrifuge (Kubota 6500, Japan) at 17,000 rpm (36,873 RCF), 4 °C for 20 min. GNP pellets were collected, re-dispersed in fresh deionized water and centrifuged twice to remove the unwanted extraneous matter and excess of coating agent. Supernatant was stored at 4 °C to study antioxidant activity by TFC, TAC and TPC. UV–Visible spectrum was recorded before and after centrifugation to confirm the purity of synthesized GNPs. Similar procedure was followed to study the effect of various process parameters like stirring (300 rpm), temperature and pH.

3.3. Characterization of GNPs

Synthesized GNPs were appropriately diluted using deionized water and wavelength scan was recorded from 700 to 200 nm by using UV–Visible spectrophotometer. Zetasizer (Malvern Instruments, UK) was used to study the particle size, particle size distribution, polydispersibility index (PDI) and zeta potential of colloidal dispersion of GNPs. Synthesized GNPs were washed with deionized water three times and lyophilized to record FT-IR (Shimadzu, Japan) spectrum by KBr pellet method. X-ray diffractometer (Philips PRO expert, Netherland) was operated at room temperature, 40 kV voltage, 30 mA current and 7^0 to 70^0 (2θ) range using nickel filtered Cu Kα radiations to record X-RD spectrum of GNPs. Scanning electron microscopy (SEM) (FEI, USA) Quanta 200 equipped with Energy dispersive X-ray Spectroscopy (EDAX) system was used to analyze GNPs. Sample was loaded on carbon grid and dried under low vacuum (10–130 pa) with a voltage of 20 keV. Initially, image was scanned at 3000×, in which a spot was fixed and analyzed by EDAX to confirm the presence of gold metal. On confirmation, images were further scanned at 6000× and 12,000× magnification and recorded. Atomic force microscopy (AFM) (Nanosurf AG, Switzerland) images were collected using a scanning probe microscope in non-contact mode with silicon nitride cantilevers under room temperature condition. GNPs were smeared over the whole slide and dried in order to get the uniform dispersed image. Transmission electron microscopy (TEM) (Hitachi H-7500, Japan) equipped with CCD camera was used to record the images. GNP colloidal sample was deposited on sample holder carbon coated copper grid and scanned at magnification of 200,000× to get the images.

3.4. Gold content estimation-inductive coupled plasma-atomic emission spectroscopy (ICP-AES) of GNPs

ICP-AES (SPECTRO ARCOS, Germany) was employed for qualitative and quantitative estimation of gold content at ppm level. Initially, calibration curve of known gold was obtained by using standard gold solution (NIST $H(AuCl_4)$ in HCl 2 mol/l 1000 mg/l Au Certipur®, Catalog no: 170,216, Merck Millipore corporation, Germany) concentrations of 0.1, 1, 10 and 100 ppm at 242.80 nm. Prior to analysis, GNPs sample (5 ml) was pre-treated with 3 ml concentrated nitric acid and heated to 75 °C for 15 min until it turns colorless. Samples were then filtered, volume was made up to 10 ml and analyzed for gold content. Instrument was controlled by a computer and the operating program was programmed using visual basic software. Experiments were performed

Table 1
Quantitative evaluation of aqueous extract.

Test	Before formation of GNPs	After formation of GNPs
Total flavonoid content μg/ml QE/g of dry extract	15 ± 1.568	5 ± 1.974
Total antioxidant capacity μg/ml of GAE/g of dry extract	85.52 ± 2.678	1.24 ± 1.689
Total phenolic content μg/ml of GAE/g of dry extract	851.9 ± 10.698	0.079 ± 1.036

All values are expressed as mean ± SD, where n = 3.

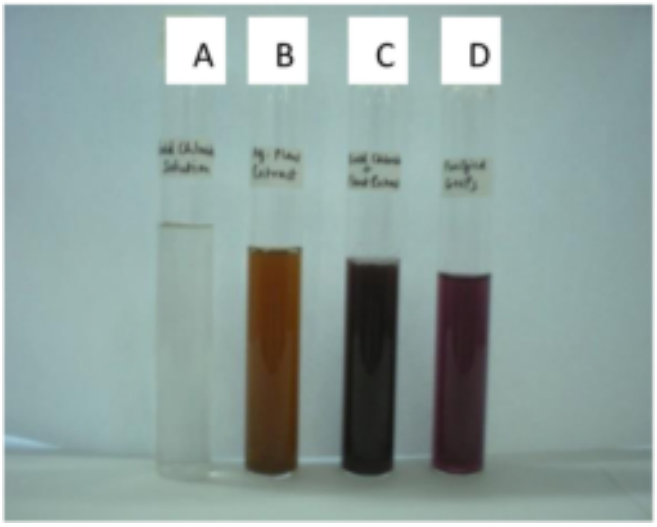

Fig. 1. Color changes after formation of GNPs from *Nepenthes khasiana*, where A) gold chloride solution B) aqueous plant extract, C) after formation of GNPs, D) after purification of GNPs.

in triplicate and results were expressed in mean (ppm) ± standard deviation.

3.5. Biocompatibility studies

3.5.1. In vitro stability studies of GNPs

In vitro stability studies were performed by mixing 1 ml of gold colloid to 0.5 ml aqueous solution each of 2% bovine serum albumin (BSA), 2% human serum albumin (HSA), 0.2 M histidine, 0.2 M cysteine, 5% NaCl, phosphate buffer pH 2, 5, 7, 10 and 12 and incubated for 30 min. Aliquots of samples were analyzed after 30 min, 24, 48, 72 h using UV–Visible spectroscopy [38].

3.5.2. Cytotoxicity evaluation of GNPs

Mouse fibroblasts (L929) cell lines were seeded in the 96 well plates at the densities of 1×10^4 cells/well/0.1 ml medium and allowed to adhere by incubating for a period of 24 h in a CO_2 incubator (Eppendorf, New Brunswick, Galaxy 170R, Germany) maintained at 37 °C and 95% humidity. The cell count was determined using a hemocytometer. The medium was discarded and replaced with fresh medium (0.1 ml) containing different concentrations of GNPs (70.3, 35.15, 17.25, 8.75 and 4.39 μg/ml) followed by incubation at 37 °C. Cytotoxicity was evaluated at predetermined time intervals of 2, 4, 12 and 24 h. The medium in each well was discarded and 50 μl of MTT solution (5 mg/ml in phosphate buffer saline) was added to each well and the plate was incubated at 37 °C. On completion of 4 h, DMSO (100 μl) was added to each well to dissolve formed formazan crystals and absorbance was recorded at 492 nm filter using ELISA plate reader (Lisa plus, India) [39] and calculated for percent cell viability.

4. Result and discussion

4.1. Preparation and evaluation of plant extract

Plant extract was prepared by simple decoction method and filtrate was used for determination of phytoconstituents. Phytochemical investigations revealed the presence of antioxidant principles like flavonoids, polyphenols, proteins, tannins and carbohydrates. Results of TFC, TPC and TAC summarized in Table 1 suggest that aqueous extract of *N. khasiana* is rich in antioxidant phytochemicals and can be used as the green source for synthesis of GNPs.

4.2. Synthesis of GNPs and effect of different parameters

Gold chloride solution when treated with plant extract at all volume ratios showed change in color from colorless to purple within 15 min as shown in Fig. 1. However, the ratio in which the GNPs were synthesized with least amount of plant extract was chosen for further studies to avoid problems associated with separation and purification of GNPs. Literature suggests that GNPs exit with colors from red to dark purple depending upon the size and shape, where red color indicates smaller particle size with predominantly spherical morphology whereas purple color indicates larger particle size with mixed morphology. Purple colored GNPs prepared by using NK had relatively larger size which was confirmed by UV–Visible spectroscopy analysis where peak was observed at 570 nm (typical band of GNPs) and TEM analysis. GNPs were purified from the extraneous matter (excess of plant extract) by filtration followed by centrifugation and analyzed by UV–Visible spectroscopy and EDAX. Comparison of UV–Visible spectra (Fig. 2) of synthesized

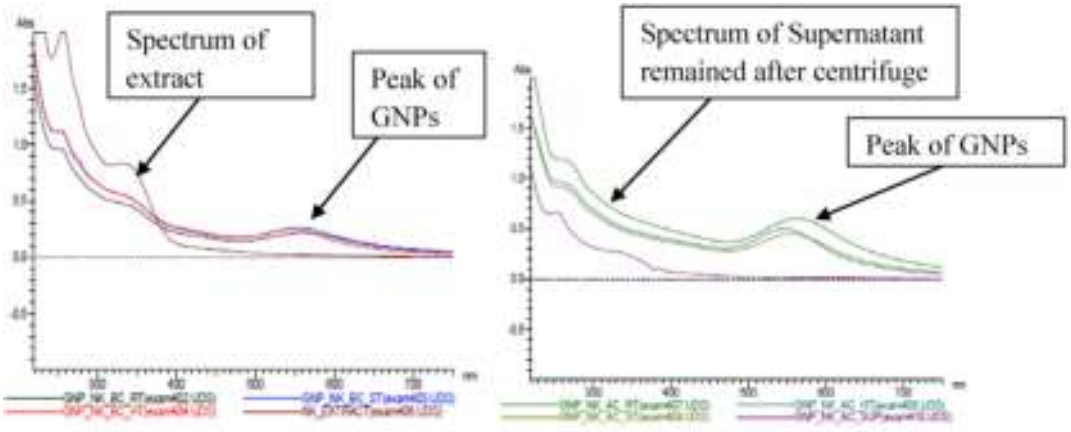

Fig. 2. Overlay UV–Visible spectra of GNPs prepared at different conditions before and after centrifuge. (GNP: gold nanoparticles, NK: *Nepenthes khasiana*, BC: before centrifuge, AC: after centrifuge, RT: room temperature, ST: stirring, HT: heating at 40 °C, SUP: supernatant remaining after centrifuge).

GNPs before and after centrifuge suggests that the synthesized GNPs are pure and free from extraneous matter.

EDAX (Fig. 3) further confirms the presence of pure elemental gold as it shows the characteristic peaks of gold metal at 2.10 and 9.50. Energy signals of carbon (C) and oxygen (O) represent the presence organic hydroxyl groups from water soluble antioxidants (polyphenols, flavonoids, proteins capping GNPs) used for synthesis of GNPs.

This validates that the phytochemicals of NK plays a key role in capping and stabilization of GNPs. Comparison of *in vitro* antioxidant assays shows that there is decrease in antioxidant potential of extract after synthesis of GNPs suggesting that antioxidant present in NK extract was utilized for preparation of GNPs. This is the first time that estimation of antioxidant potential was performed quantitatively to confirm their role in synthesis of GNPs. Results of antioxidant assays (Table 1) confirm that phytochemicals mainly flavonoids, polyphenols and other antioxidant principles are responsible for synthesis of GNPs. Literature suggests that carbohydrates, polyphenols, tannins and flavonoids act as a natural reducing agent for synthesis of GNPs and proteins act as a stabilizing agent [25].

Similarly GNPs were also synthesized by altering the process parameters like temperature, agitation and pH. In all conditions, 10:1 volume ratio of gold chloride solution to plant extract was found to be optimized in all experiments in which a color change from colorless to purple was observed. The color change arises because of the coherent oscillation of free conduction electrons induced by the interacting electromagnetic field at the surface of GNPs resulting in surface plasmon resonance [25]. It was observed that stirring and heating increase the rate of reaction which was evident by the reduction in the time taken for synthesis of GNPs. Time taken for synthesis of GNPs was in the order as room temperature (RT) (15 min) > stirring at room temperature (ST) (8 min) > heating (HT) (5 min). Synthesis of GNPs using NK requires around 5 min suggesting that it is one of the fastest methods for the synthesis for GNPs. This fast synthesis may be due to high content of antioxidants in NK and the application of heat (40 °C) which acts as the catalyst and potentiates rapid synthesis of GNPs.

Further, the effect of different pH conditions (pH 2, 7 and 10) showed that there was formation of purple color at neutral pH, florescence purple color at alkaline pH and no color in acidic condition. This suggests that synthesis of GNPs was obtained only at neutral pH conditions. Further, UV–Visible spectroscopy confirms the formation of GNPs in neutral condition whereas in alkaline condition though the peak was observed, it was broad suggesting polydispersed particles, hence was not studied for further analysis. Contradictorily, Ghodake et al. suggest that alkaline condition served as a high yielding medium for synthesis of GNPs, in which the reason was attributed to the presence of alkaline responsive phytochemicals present in pear fruit [40]. This suggests that phytochemicals play a vital role in exploiting the medium for synthesis of GNPs.

Comparing biological methods, it is reported that NADH-dependent reductase from fungus [17] or mitroreductace from enterobacteria [41] reduces metallic salts corresponding to metallic nanoparticles, whereas terpenoids, flavonoids, carbohydrates, proteins etc. present in plant extracts are responsible for reduction and stabilization of nanoparticles [42]. Literature also suggests that almost all plants are capable for synthesis and stabilization of GNPs, albeit with different reduction rate, different size, different morphology and different stability characteristics.

4.3. Characterization of GNPs

Characterization was carried out to confirm the formation of GNPs and to study its surface morphology and stability as summarized in Table 2. UV–Visible peak of gold colloid at 570 nm confirms the successful formation of GNPs and reached saturation within 15 min of reaction. Peak positions of UV–Visible spectra are mainly influenced by particle shape, dielectric constant of medium and temperature [43] and suggest the polydispersibility of synthesized GNPs. The asymmetrical and broad SPR bands indicate the formation of anisotropic GNPs. In the present

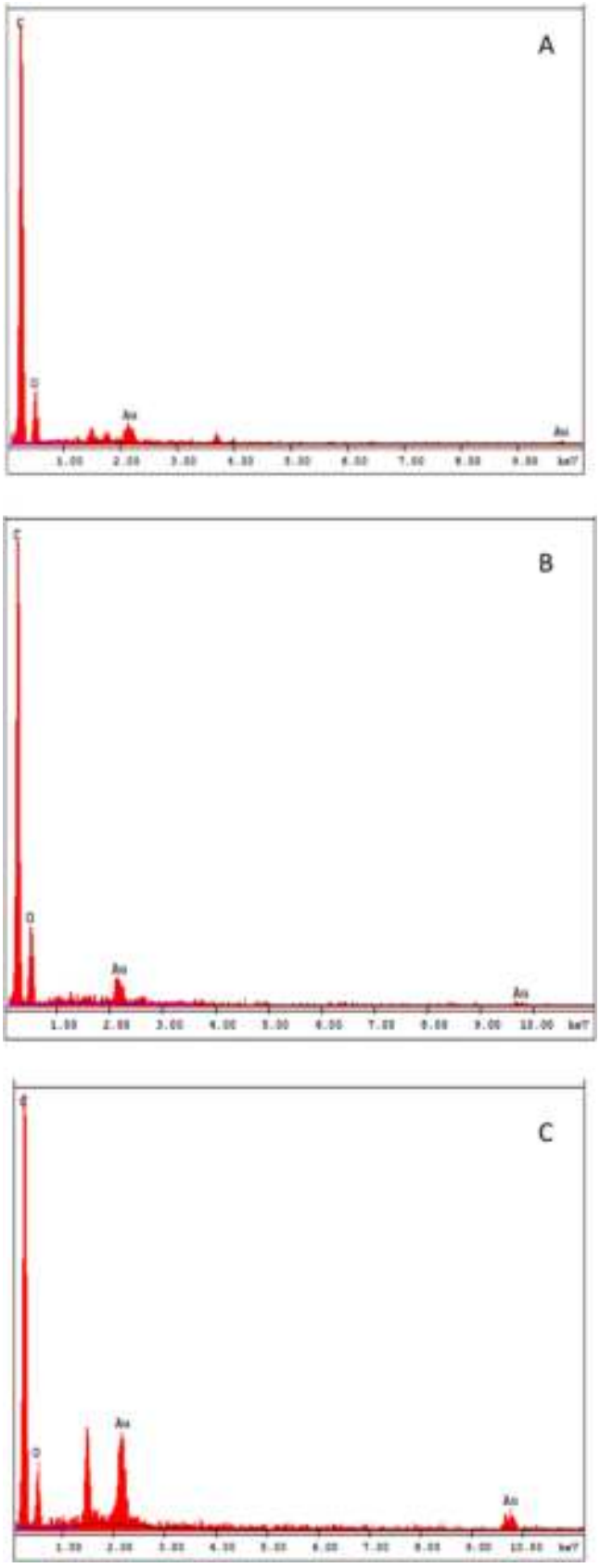

Fig. 3. EDAX spectra of GNPs prepared A) at room temperature B) by stirring C) by heating (40 °C).

Table 2
Comparative data for synthesis of GNPs at different conditions.

Synthesis of GNPs using extract of NK			
Conditions →	Room temperature (~ 30 °C)	Stirring	Heating
Characteristics ↓			
Solvent used	Deionized water	Deionized water	Deionized water
Reaction temperature	~ 30 °C	~ 30 °C	40 °C
Reaction time [in minutes	15 ± 4	8 ± 3	5 ± 2
Stability	Stable	Less stable	Stable
Bio-compatibility	Suitable for *in vivo* experiments	Suitable for *in vivo* experiments	Suitable for *in vivo* experiments
Eco-compatibility	No chemicals used	No chemicals used	No chemicals used
Particle size (nm)	178.33 ± 8.79	151.95 ± 1.08	127.36 ± 1.96
Poly dispersity index	0.419 ± 0.029	0.294 ± 0.03	0.236 ± 0.02
Zeta potential (mV)	−22.8 ± 0.7	−15.8 ± 1.35	−23.1 ± 0.15

All values are expressed as mean ± SD, where n = 3.

study, it was observed that at room temperature, 15 min was required whereas earlier studies have shown 1 h [26] or more for formation of GNPs. This confirms that the present method for synthesis of GNPs is the fastest method. Analysis by UV–Visible spectra reveals that the GNPs synthesized at room temperature and heating (40 °C) showed narrow peak when compared to the stirring and alkaline conditions in which the peaks were broad as shown in Fig. 2. The reaction rate was directly proportional to the temperature leading to formation of the primary nuclei of GNPs, thereby avoiding the secondary reduction process on the surface of the preformed nuclei [26]. Narrow peak confirms the presence of predominantly spherical GNPs whereas broad peak confirms the presence of polydispersed and polymorphic GNPs which was further supported by TEM analysis as shown in Fig. 4. However, these results are not in consensus with Aromal et al. which says that GNPs synthesized at higher temperature showed broad UV–Visible peaks. These broad peaks (suggesting increase in particle size) might be due to overheating or heating at higher temperature (100 °C) for longer time [14]. Proteins present in the plant extract are mainly responsible for stabilization of GNPs. These proteins might get denatured at higher temperature thereby causing aggregation and increase in particle size of GNPs [44].

GNPs were centrifuged at 17,000 rpm for 20 min and the pellets were washed thrice with deionized water to get rid of the free proteins and enzymes that are not coating the GNPs. The samples were dried (lyophilized) and grinded with KBr pellets and analyzed by FT-IR spectroscopy. FT-IR spectra show the presence of peaks at 3321 cm^{-1}, 3145 cm^{-1}, 2920 cm^{-1}, 1614 cm^{-1} and 1259 cm^{-1} as shown in Fig. 5. These peaks confirm the presence of organic functional groups of phytochemicals like flavonoids, polyphenols and proteins which are responsible for formation and stabilization of GNPs. Peak at 3321 cm^{-1} represents —OH stretching vibrations which confirms the presence of hydroxyl group, 3145 cm^{-1} and 2920 cm^{-1} represent—C—H stretching, due to the presence of methyl, methoxy and methylene group, 1614 cm^{-1} represents the presence of —C═O group of carboxylic acid, 1259 cm^{-1} shows amide band of polypeptide and proteins and 1078 cm^{-1} further confirms the presence of amide group. Presence of these peaks represents different phytochemicals present in NK like peptides/proteins, terpenoids, aldehydes/ketones, tartaric acid, alkaloids, and flavonoids coated onto GNPs during reduction process and is mainly responsible for stabilization of GNPs. FT-IR data was also supported by *in vitro* antioxidant assays like TFC, TPC and TAC performed before and after formation of GNPs.

All the reflection peaks at 38.4, 44.24 and 64.5 in XRD spectra as shown in Fig. 6 correspond to face-centered cubic gold with (111), (002) and (022) which suggests that the synthesized GNPs were nanocrystalline in nature.

There are two types of diameter of metallic nanoparticles, one actual diameter and the other is hydrodynamic diameter. Analytical methods used for determination of actual diameter are TEM, AFM and SEM whereas the hydrodynamic diameter can be determined by using DLS method.

DLS studies revealed that the particle size (hydrodynamic diameter) of GNPs was in the range of 125–180 nm. Negative zeta potential of GNPs prepared at room temperature, stirring and heating are −22.8 ± 0.7, −15.8 ± 1.35 and −23.1 ± 0.15 respectively. Zeta potential is defined as the measurement of charge and is the most important determinant for the stability of GNPs. Magnitude of zeta potential is the indicative of the balance between the repulsive and attractive forces between GNPs. Stability is directly proportional to the magnitude of repulsive forces and inversely proportional to the attractive forces between GNPs. Hence it was confirmed that the GNPs synthesized were disperse

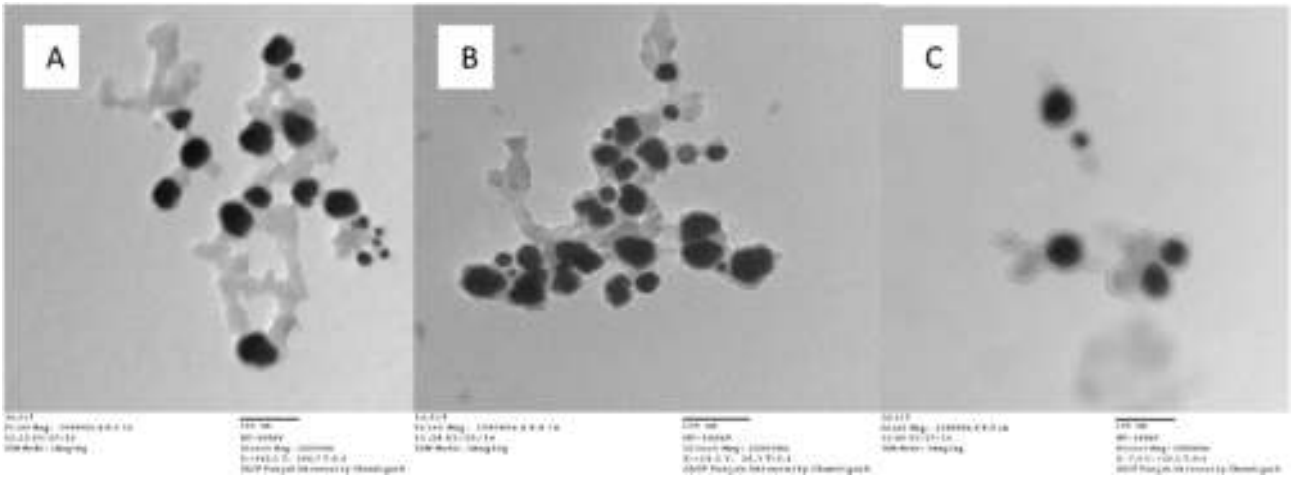

Fig. 4. TEM images of GNPs prepared A) at room temperature B) by stirring C) by heating (40 °C).

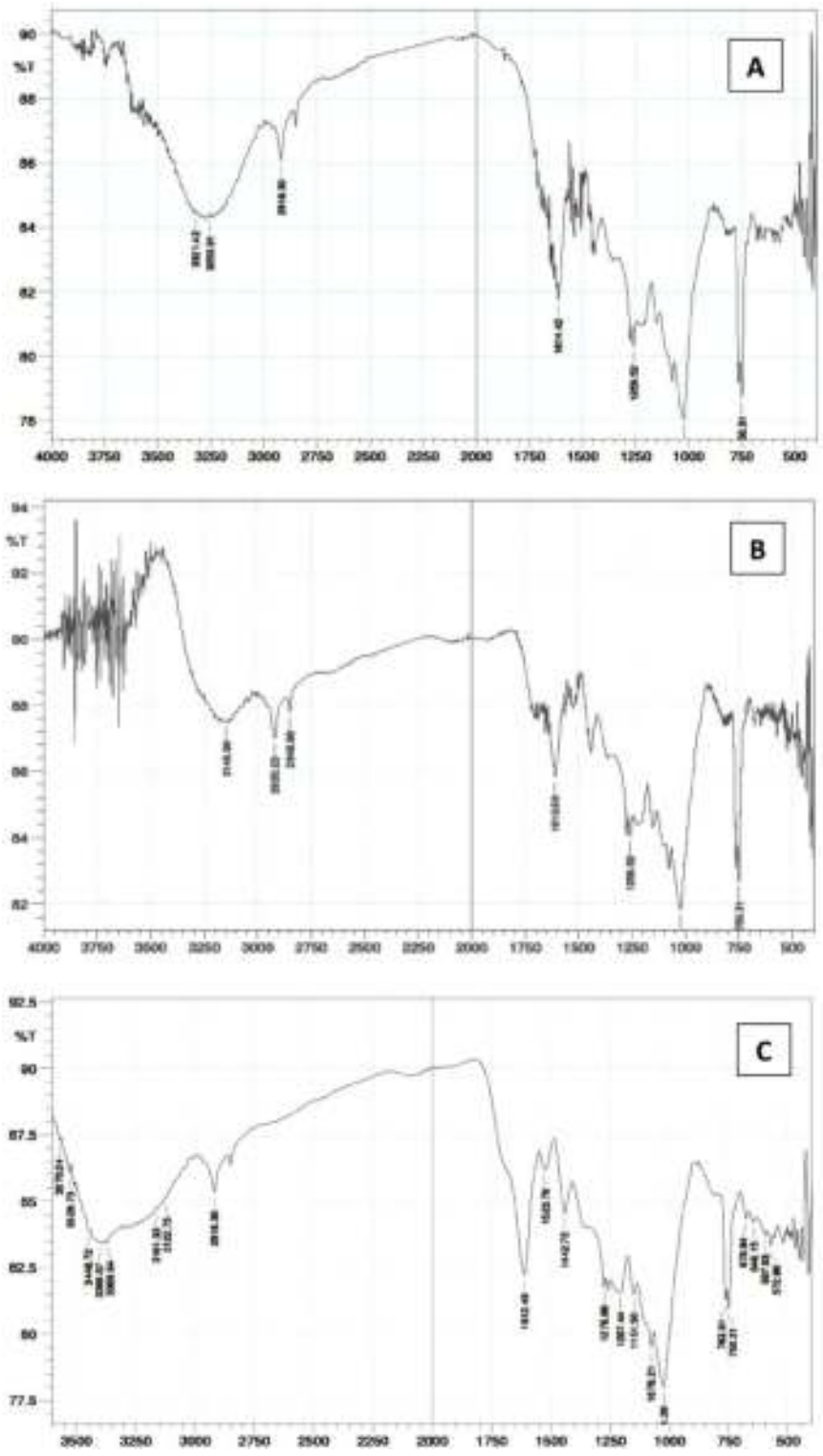

Fig. 5. FT-IR spectra of GNPs prepared A) at room temperature B) by stirring C) by heating (40 °C).

and stable. Negative zeta potential could be due to the hydroxyl group containing phytochemicals present in NK used for reducing and stabilizing the GNPs. These phytochemicals are responsible for providing a robust coating on GNPs and thus, rendering stability against aggregation. Shape and size of stabilized nanoparticles are important aspects of nanoformulation as they play a vital role in modulating their optical properties [25]. Ankamwar [45] synthesized anisotropic planner GNPs with triangular morphology for vapor sensing applications whereas gold triangles synthesized using lemon grass are used in hyperthermia of tumors.

Determination of surface morphology and elemental identification of GNPs was performed by using SEM coupled with EDAX. Results of SEM analysis as shown in Fig. 7 suggest that the GNPs synthesized in all conditions are dispersed while EDAX clearly shows the presence of sharp peak of gold metal suggesting the purity of GNPs.

AFM has proved to be an important biophysical technique for determining the surface topography of GNPs [46]. The understanding of the functionalization of the GNPs synthesized extracellularly using extract of NK was confirmed by AFM (Fig. 8) which clearly shows rich concentration

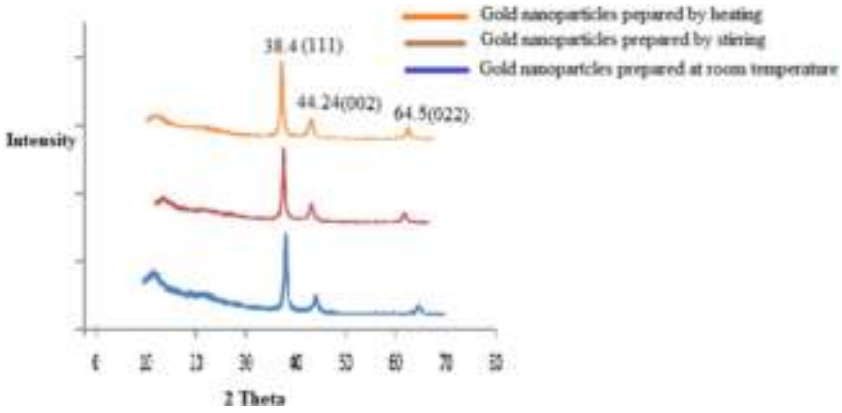

Fig. 6. X-RD spectra of GNPs prepared A) at room temperature B) by stirring C) by heating (40 °C).

of organic moieties coated onto GNPs. AFM image of GNPs prepared at RT, ST and HT shows a clear difference in surface topography in which RT showed a smooth surface with bigger size, ST generated GNPs with comparatively smaller size with rough surface and HT showing smallest size with gritty and rough surface when compared to RT and ST. The surface topography revealed a homogeneously distributed arrangement of nano-sized GNPs, with most of the particles assembled transversely. Results of AFM were in line with SEM and DLS which shows predominant spherical GNPs.

To obtain higher resolution clear morphology of GNPs, TEM was used which showed distorted spherical morphology of GNPs synthesized in all conditions. TEM images as shown in Fig. 4 also suggest that the GNPs synthesized at RT and HT (40 °C) are smaller in size when compared with the particle size of GNPs synthesized by ST. TEM shows that coating agent is smooth and uniform in GNPs synthesized by HT and RT whereas ST leads to removal of coating agent. Nanocrystals devoid of shielding/coating biomolecules were thermodynamically unstable. The spherical nanoparticles produced in the beginning of the reaction were stable due to the protection by sufficient biomolecules. The newly shaped nanotriangles suffered a shrinking process to reduce their high surface energy to a minimum resulting in the formation of truncated morphologies from sharp angles structures [25]. It was also observed from TEM analysis that GNPs synthesized at RT were having mixed morphology, whereas GNPs synthesized at HT (40 °C) showed predominantly distorted spherical morphology. It is believed that at higher temperature, gold ion first forms nuclei and the

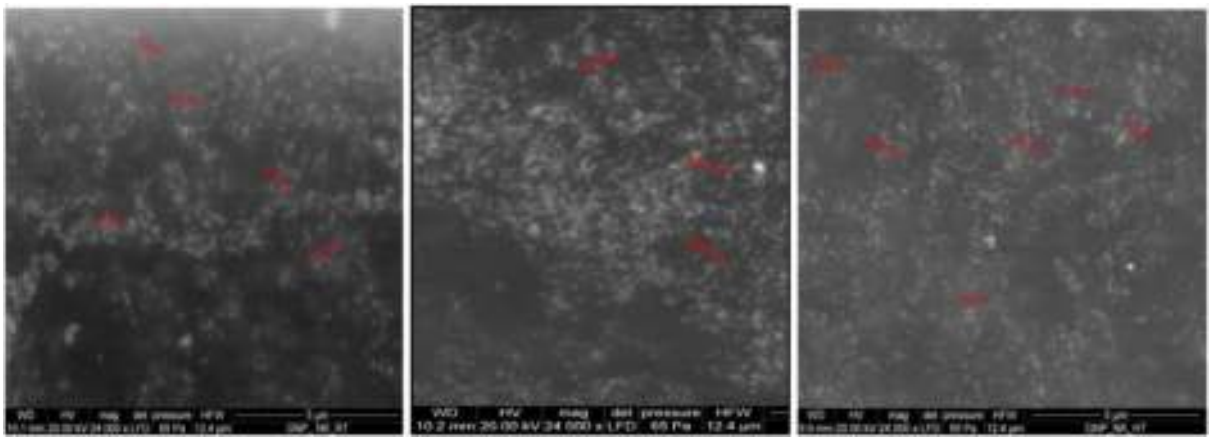

Fig. 7. SEM images of GNPs prepared A) at room temperature B) by stirring C) by heating (40 °C).

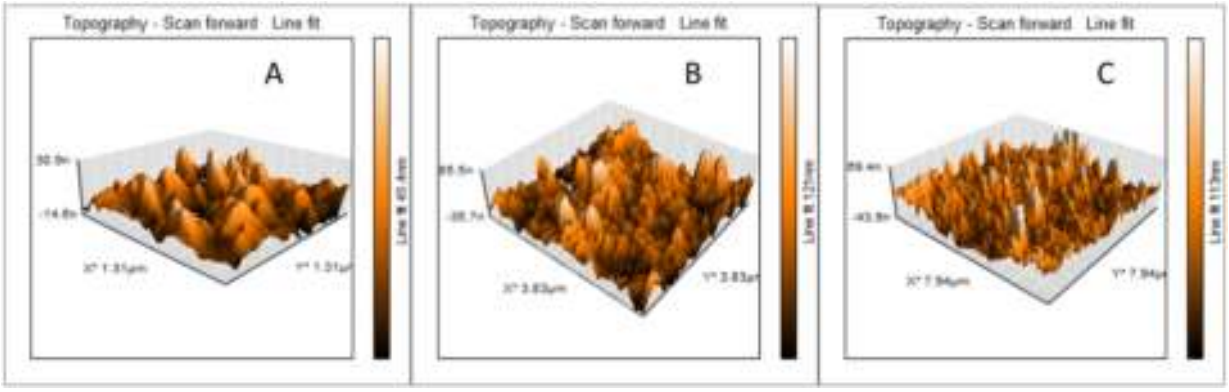

Fig. 8. AFM image of GNPs prepared A) at room temperature B) by stirring C) by heating (40 °C).

secondary growth of particle stops because the rate of the reaction is very fast when the reaction is heated [26].

4.4. ICP-AES—gold content estimation

Calibration curve was plotted by using standard concentrations of gold in the range of 0.1 to 100 mg/ml. The calibration graph for gold was linear at ppm level concentrations in which the correlation coefficient of the calibration curve of silver was 0.999. Samples on treatment with nitric acid were found to be colorless and warranted that the gold is completely solubilized in solution. The concentration of synthesized GNPs measured by using ICP-AES was found to be 70.3 ± 6.2 μg/ml.

4.5. Biocompatibility studies of GNPs

4.5.1. In vitro stability studies of GNPs

In vitro stability studies also known as blood compatibility studies was performed to confirm the stability of green synthesized GNPs on exposure to various blood components and different pH conditions over a reasonable period of time. Stable GNPs were tested against 0.2 M cysteine, 0.2 M histidine, 2% bovine serum albumin (BSA), 2% human serum albumin (HSA), 5% NaCl, phosphate buffer pH 2, 5, 7, 10 and 12. Cysteine—a natural amino acid present in blood has a potential thiol functional group capable for exchanging with the coating material of GNPs leading to unstability. On the other hand histidine—a natural amino acid present in blood is mainly responsible to trigger the immune response to allergens in the body. Hence, testing of GNPs against histidine was performed with a view to confirm the resistivity of GNPs to avoid triggering of an immune reaction in the body which might interfere with the target specificity of stable GNPs. From the various blood components, albumin is abundantly available, which established the base to test GNPs against plasma proteins like BSA (mammals) and HSA (humans). For various *in vivo* biodistribution studies, GNPs are supposed to be injected intravenously which makes it mandatory that the GNPs should be stable/intact in blood during animal testing. Similarly, GNPs should retain their stability and morphology after i.v. administration in human subjects as in case of animal models. GNPs were tested against the electrolyte solution (5% NaCl) which is available in clinical settings as saline (0.9% NaCl) and generally used as the diluent or adjutant to intravenous therapies. Moreover, presence of Na + and K + ions are abundant in cellular systems and are well known to aggregate in the presence of electrolytes [38,47].

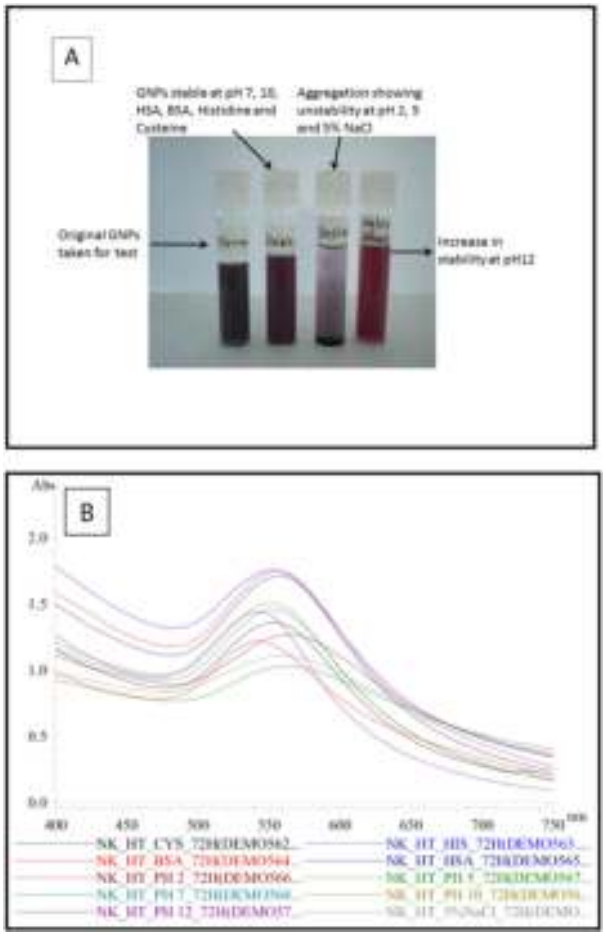

Fig. 9. A: Photograph depicting color of GNPs on exposure to various blood components and different pH; B: UV–Visible Spectra and photograph showing *in vitro* stability studies of GNPs in blood components (GNP: gold nanoparticles, NK: *Nepenthes khasiana*, RT: room temperature, ST: stirring, HT: heating at 40 °C, CYS: cysteine, HIS: histidine, BSA: bovine serum albumin, HSA: human serum albumin).

The shift of SPR peak by 5 nm wavelength in all the above mixtures was permissible and recognized as stable and intact GNPs. Stability studies revealed that the GNPs were stable in all conditions except in acidic pH and 5% NaCl where red shift was observed (Fig. 9B) suggesting increase in particle size followed by aggregation leading to instability. In alkaline condition (pH 12), GNPs were found to be more stable than original GNPs (control GNPs taken for stability studies). It can be observed from SPR studies which demonstrate a remarkable blue shift from 570 nm to 555 nm indicating the decrease in size of GNPs. The photograph depicted in Fig. 9A shows a red color (highly stable) instead of purple color (original NK synthesized GNPs). These results are in corroboration with the existing literature which suggests that increase in pH enhances the homogenous nucleation and decrease in anisotropic growth of GNPs whereas acidic condition results in slow processing and generation of secondary nucleation on existing gold seeds. Moreover, alkaline condition tends to generate more of negatively charged hydroxyl ions (OH^-) which interact with the existing negative charge on surface of GNPs giving rise to electrostatic force of repulsion subsequently generating higher Brownian moments to create extra stable GNPs [48]. This mechanism was supported by zeta potentiometric results which show that zeta potential of original GNPs as −22.8 ± 0.7 and −30.6 ± 1.14 for GNPs exposed to pH 12. However, acidic pH generated positively charged hydrogen ions (H^+) which reacted with negatively charged surface of GNPs decreasing the electrostatic force between GNPs leading to aggregation and unstability [49]. The stability of GNPs colloidal dispersion is determined by the balance of the repulsive and attractive forces that occur between GNPs as they approach one another. Dispersion is said to be stable when the repulsive forces overcome attraction forces keeping the particles dispersed in dispersion medium leading to stable colloid. However, little or no repulsion between particles, leads to aggregation. In other words, the use of simulated/alkaline solution may be a new way for formulators to regulate the shape and size of GNPs by merely varying the pH value of the reaction mixture.

GNPs synthesized in the present research investigation can be used for various biomedical applications but at very lower concentrations. So, it was essential to test if dilutions of NK stabilized GNPs alter its chemical and photo-physical properties. To determine the stability of GNPs under dilution, the UV–Visible wavelength was examined after every sequential addition of 0.2 ml of ionized water to 1 ml of GNPs colloidal dispersion. The absorption intensity at 570 nm wavelength was found to be linearly proportional on the concentration of GNPs and obeyed Beers Lamberts law. It was also observed that the wavelength of GNPs remained constant at 570 nm throughout the experiment at dilutions in the range of 10^{-5} to 10^{-6} ml as these are typical concentrations used at cellular levels [39,50,51].

4.5.2. Cytotoxicity evaluation of GNPs

Biocompatibility is the important parameter to be evaluated for any nanomaterial intended for *in vivo* biomedical applications.

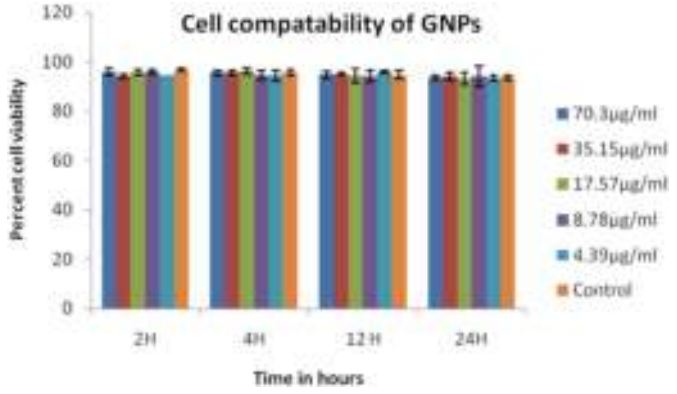

Fig. 10. Biocompatibility studies of GNPs using MTT assay against mouse fibroblasts (L929) cell lines.

Biocompatibility of nanoformulation is studied by evaluating the potential cytotoxicity against normal cell lines. In the present investigation, cytotoxicity of NK stabilized GNPs in primary mouse fibroblast cultures was evaluated as *in vitro* experimental models based on MTT assay. Fibroblast cells were treated with GNPs at concentrations of 70.3, 35.15, 17.25, 8.75 and 4.39 µg/ml and evaluated cell viability after 2, 4, 8, 12 and 24 h using colorimetric MTT (methyl thiazolyl tetrazolium) assay. Cytotoxicity of samples was compared with control (untreated) cells that were considered as 100% viable (Fig. 10)

It was found that green synthesized GNPs were biocompatible and non-cytotoxic even at higher concentrations. Literature reveals that a number of gold complexes, salt and derivatives have demonstrated significant cytotoxicity [50,51]. Different concentrations of GNPs selected for study of biocompatibility studies were dependent on various biomedical applications [52]. The synergistic reduction capabilities of phytochemicals in Nepenthes that efficiently reduced gold salt in aqueous media comply with the fundamental principles that govern green chemistry. This green nanotechnology approach is distinctive because the GNPs are not only synthesized but also simultaneously stabilized by the phytochemicals present in plant extract. It is worth to note that phytochemicals, proteins and carbohydrates ensure reduction of gold salt to corresponding GNPs, in which the group of proteins and peptides along with antioxidants phytochemicals in NK effectively coat GNPs to render excellent robustness against aggregation. The present investigation reports that plant based chemicals are of vital importance in context of synthesis of GNPs for *in vivo* biomedical applications under nontoxic conditions. Lack of any toxicity of NK stabilized GNPs provides new prospects for the safe delivery and applications of such nanoparticles in targeted therapy and molecular imaging.

5. Conclusion

Functionalized, charged, biocompatible and stable GNPs play a crucial role in the overall research and development of GNPs based nanomedicine. Current method of synthesis requires only gold chloride as precursors and no man-made chemicals were used in the complete fabrication process. This further asserts that there are consequently no harsh chemicals employed in the synthesis or harsh by products formed during synthesis. Processes involved are therefore eco-friendly and biologically benign in which stabilized, biocompatible GNPs will require no further treatment prior to its biomedical application. These performance necessities will enforce stern restrictions on the use of synthetic chemicals used for synthesis of GNPs. *Nepenthes khasiana* NK mediated GNPs were successfully synthesized and study of different process parameters like effect of pH, stirring and temperature is demonstrated. During synthesis, heating at lower temperature (40 °C) yields GNPs with better stability characteristics and desirable zeta potential. Absence of cytotoxicity against mouse fibroblasts and *in vitro* stability studies in blood components confirms biocompatible nature of GNPs. Antioxidant phytochemicals mainly polyphenols, flavonoids, and proteins not only result in efficient reduction of gold chloride to GNPs but their chemical structure coat around the GNPs to render exceptional robustness against aggregation. Present studies described herein serve as a distinctive illustration of the tendency of the phytochemicals in NK to reduce gold salt to GNPs. Synthesized biocompatible and stable GNPs are suitable for *in vivo* biomedical applications via direct administration into human tissues through intravenous route. GNPs owning to their opaque nature to X-rays can provide an unprecedented contrast between the cancerous and healthy tissues when observed through X-ray computer tomography scans. They could also be used for treatment of targeted tissues by localized hyperthermia, coating of hairs and skin. This one pot green synthesis was found to be effective for the synthesis and stabilization of biocompatible GNPs and provide unique prospects toward the formulation and development of well-designed green GNPs that can be safely synthesized, stored and marketed globally.

Acknowledgements

Authors wish to acknowledge KLE University and Regional Medical Research Centre—Indian Council of Medical Research (ICMR), Belgaum for providing facility to carry out the research. We also thank SAIF, Panjab University, Chandigarh for TEM and SAIF, Indian Institute of Technology (IIT), Bombay for ICP-AES analysis.

References

[1] L. Jing-Liang, L. Wang, L. Xiang-Yang, Z. Zhang, G. Hong-Chen, L. Wei-Min, et al., In vitro cancer cell imaging and therapy using transferrin-conjugated gold nanoparticles, Cancer Lett. 27 (2) (2009) 319.
[2] R.A. Sperling, P.R. Gil, F. Zhang, M. Zanella, W.J. Parak, Biological applications of gold nanoparticles, Chem. Soc. Rev. 37 (2008) 1896.
[3] F. Kim, S. Connor, H. Song, T. Kuykendall, P. Yang, Platonic gold nanocrystals, Angew. Chem. 116 (2004) 3759.
[4] D. Raghunandan, S. Basavaraja, B. Mahesh, S. Balaji, S.Y. Manjunath, A. Venkataraman, Biosynthesis of stable polyshaped gold nanoparticles from microwave-exposed aqueous extracellular anti-malignant guava (*Psidium guajava*) leaf extract, Nanobiotechnol. 5 (2009) 34–41.
[5] R.R. Naik, S.J. Stringer, G. Agarwal, S.E. Jones, M.O. Stone, Bio-mimetic synthesis and patterning of silver nanoparticles, Nat. Mater. 1 (2002) 169–172.
[6] K.H. Magnusson, K. Deppert, J.O. Malm, J.O. Bovin, L. Samuelson, Size-selected gold nanoparticles by aerosol technology, Nanostruct. Mater. 12 (1999) 45–48.
[7] F. Mafune, J. Kohono, Y. Takeda, T. Kondow, Full physical preparation of size-selected gold nanoparticle in solution: laser ablation and laser induced size control, J. Phys. Chem. B 106 (2002) 7575–7577.
[8] K. Okitsu, A. Yue, S. Tanabe, H. Matsumoto, Y. Yobiko, Formation of colloidal gold nanoparticles in an ultrasonic field: control of rate of gold (III) reduction and size of formed gold particles, Langmuir 17 (2001) 7717–7720.
[9] T.K. Sau, A. Pal, N.R. Jana, Z.L. Wang, T. Pal, Size controlled synthesis of gold nanoparticles using photochemically prepared seed particles, J. Nanoparticle Res. 3 (2001) 257–261.
[10] W.M. Tolles, Nanoscience and nanotechnology in Europe, Nanotechnology 7 (1996) 59–105.
[11] K. Esumi, A. Kameo, A. Suzuki, K. Torigoe, T. Yoshimura, Y. Koide, et al., Preparation of gold nanoparticles using 2-vinylpyridine telomers possessing multi-hydrocarbon chains as stabilizer, Colloids Surf., A 176 (2001) 233–237.
[12] S.L. Westcott, N.J. Halas, S.J. Oldenburg, T.R. Lee, Formation and adsorption of clusters of gold nanoparticles onto functionalized silica nanoparticle surfaces, Langmuir 14 (1998) 5396–5401.
[13] M.Y. Han, C.H. Quek, W. Huang, C.H. Chew, L.H. Gan, A simple and effective chemical route for the preparation of uniform nonaqueous gold colloids, Chem. Mater. 11 (1999) 1144–1147.
[14] S. Aromal, V. Vidhu, D. Philip, Green synthesis of well-dispersed gold nanoparticles using *Macrotylomauniflorum*, Spectrochim. Acta A Mol. Biomol. Spectrosc. 85 (1) (2011) 99–104.
[15] N. Wang, Y. Cai, R. Zhang, Growth of nanowires, Mater. Sci. Eng. R 60 (2008) 1–5.
[16] A. Ahmad, S. Senapati, M.I. Khan, R. Kumar, M. Sastry, Extracellular biosynthesis of monodisperse gold nanoparticles by a novel extremophilic actinomycete, Thermomonospora sp, *Langmuir* 19 (8) (2003) 3550–3553.
[17] P. Mukherjee, S. Senapati, D. Mandal, A. Ahmad, M.I. Khan, R. Kumar, M. Sastry, Extracellular synthesis of gold nanoparticles by the fungus *Fusarium oxysporum*, Chembiochem 3 (5) (2002) 461–463.
[18] N. Durán, D. Priscyla, M. Durán, A. Yadav, A. Gade, M. Rai, Mechanistic aspects in the biogenic synthesis of extracellular metal nanoparticles by peptides, bacteria, fungi, and plants, Appl. Microbiol. Biotechnol. 90 (5) (2011) 1609–1624.

[19] A.S. Reddy, C. Chien-Yen, C. Chien-Cheng, J. Jiin-Shuh, C. Hau-Ren, T. Min-Jen, F. Cheng-Wei, W. Jung-Chen, Biological synthesis of gold and silver nanoparticles mediated by the bacteria *Bacillus subtilis*, J. Nanosci. Nanotechnol. 10 (10) (2010) 6567–6574.
[20] Y. Konishi, T. Takeshi, O. Kaori, S. Norizoh, N. Toshiyuki, N. Shinsuke, Intracellular recovery of gold by microbial reduction of AuCl 4 − ions using the anaerobic bacterium *Shewanella algae*, Hydrometallurgy 81 (1) (2006) 24–29.
[21] M. Gericke, A. Pinches, Microbial production of gold nanoparticles, Gold Bull. 39 (2006) 22–28.
[22] M. Labrenz, G.K. Druschel, T. Thomsen-Ebert, B. Gilbert, S.A. Welch, K.M. Kemner, G.A. Logan, R.E. Summons, G. De Stasio, P.L. Bond, B. Lai, S.D. Kelly, J.F. Banfield, Formation of sphalerite (ZnS) deposits in natural biofilms of sulphate reducing bacteria, Science 290 (2000) 1744–1747.
[23] J.L. Gardea-Torresdey, J.G. Parsons, E. Gomez, J. Peralta-Videa, H.E. Troiani, P. Santiago, et al., Plants with the Midas touch: formation of gold nanoparticles by alfalfa plants, Nano Lett. 2 (2002) 397–401.
[24] N.C. Sharma, S.V. Sahi, S. Nath, J.G. Parsons, J.L. Gardea-Torresdey, T. Pal, Synthesis of plant-mediated gold nanoparticles and catalytic role of biomatrix-embedded nanomaterials, Environ. Sci. Technol. 15 (2007) 5137–5142.
[25] B.K. Narayanan, N. Sakthivel, Phytosynthesis of gold nanoparticles using leaf extract of *Coleus amboinicus* Lour, Mater. Charact. 61 (11) (2010) 1232–1238.
[26] J.Y. Song, J. Hyeon-Kyeong, S.K. Beom, Biological synthesis of gold nanoparticles using *Magnolia kobus* and *Diopyros kaki* leaf extracts, Process Biochem. 44 (10) (2009) 1133–1138.
[27] M. Han, X. Gao, J.Z. Su, S. Nie, Quantum-dot tagged microbeads for multiplexed optical coding of biomolecules, Nat. Biotechnol. 19 (2001) 631–635.
[28] M. Moreno-Manas, R. Pleixats, Formation of carbon-carbon bonds under catalysis by transition-metal nanoparticles, Acc. Chem. Res. 36 (2003) 638–643.
[29] C.N.R. Rao, A.K. Cheetham, Science and technology of nanomaterials: current status and future prospects, J. Mater. Chem. 11 (2001) 2887–2894.
[30] A. Alivisatos, P. Perspectives on the physical chemistry of semiconductor nanocrystals, J. Phys. Chem. 100 (1996) 13226–13239.
[31] J. Aizpurua, P. Hanarp, D.S. Sutherland, M. Kall, G.W. Bryant, D.A.J. Garcia, Optical properties of gold nano rings, Phys. Rev. Lett. 5 (2003) 057401.
[32] R. Jin, Y. Cao, C.A. Mirkin, Photo induced conversion of silver nanospheres to nanoprism, Science 294 (2001) 1901–1903.
[33] M.A. El-Sayed, Some interesting properties of metals confined in time and nanometer space of different shapes, Acc. Chem. Res. 34 (2001) 257–264.
[34] S.H. Huang, Gold nanoparticles-based immune chromatographic test for identification of *Staphylococcus aureus* from clinical specimens, Clin. Chim. Acta 373 (2006) 139–143.
[35] Environmental information system, *envis.* frlht.org/junc**list**.php, downloaded at 6.10.2014 at 19:51.
[36] R.G. Singh, P. Negi, C. Radha, Phenolic composition, antioxidant and antimicrobial activities of free and bound phenolic extracts of *Moringa oleifera* seed flour, J. Funct. Foods 5 (4) (2013) 1883–1891.
[37] B. Moyo, S. Oyedemi, P. Masika, V. Muchenje, Polyphenolic content and antioxidant properties of *Moringa oleifera* leaf extracts and enzymatic activity of liver from goats supplemented with *Moringa oleifera* leaves/sunflower seed cake, Meat Sci. 91 (4) (2012) 441–447.
[38] Katti, K. Kannan, R. and Katti, K. Stabilized, biocompatible gold nanoparticles and environ-friendly method for making same, US patent 2009/0074674 A1, March 19 2009.
[39] D. Menon, A. Basanth, A. Retnakumari, K. Manzoor, S.V. V. Nair, Green synthesis of biocompatible gold nanocrystals with tunable surface plasmon resonance using garlic phytochemicals, J. Biomed. Nanotechnol. 8 (2012) 901–911.
[40] G. Ghodake, N. Deshpande, Y. Lee, E. Jin, Pear fruit extract-assisted room-temperature biosynthesis of gold nanoplates, Colloids Surf. B: Biointerfaces 75 (2010) 584–589.
[41] H.R. Shahverdi, R. Ahmad, M. Sara, H. Jamalifar, N. Ashraf-Asadat, Rapid synthesis of silver nanoparticles using culture supernatants of Enterobacteria: a novel biological approach, Process Biochem. 42 (5) (2007) 919–923.
[42] S. Shankar, A.A.R. Shiv, A. Ahmad, M. Sastry, Rapid synthesis of Au, Ag, and bimetallic Au core–Ag shell nanoparticles using neem (*Azadirachta indica*) leaf broth. J. Colloid Interface Sci. 275 (2) (2004) 496–502.
[43] A.C. Templeton, J.J. Pietron, R.W. Murray, P. Mulvaney, Solvent refractive index and core charge influences on the surface plasmon adsorbance of alkane thiolate monolayer-protected gold clusters, J. Phys. Chem. B 104 (2000) 564–570.
[44] U. Satyanarayana, U. Chakrapani, Biochemistry, Proteins and Amino Acids, fourth ed.61 Elsevier Publications, India, 2013.
[45] B. Ankamwar, M. Chaudhary, S. Murali, Gold nanotriangles biologically synthesized using tamarind leaf extract and potential application in vapor sensing, Synth React Inorg Met-org Nanometal Chem 35 (2005) 19–26.
[46] B.B. Robert, J.B. David, L.J. Toca-Herrera, A.W. Blake, D.A. Smith, S.E. Radford, et al., Force mode atomic force microscopy as a tool for protein folding studies, Anal. Chim. Acta 479 (1) (2003) 87.
[47] Keene, M. Athena, P. David, R. Rodney, S. Sharron, T.R. Elliot, M.T. Katherine, Tissue and cellular distribution of gold nanoparticles varies based on aggregation/agglomeration status, *Nanomedicine* 7 (no. 2) (2012) 199–209.
[48] G. Zhan, H. Jiale, L. Liqin, L. Wenshuang, E. Kamana, L. Qingbiao, Synthesis of gold nanoparticles by Cacumen Platycladi leaf extract and its simulated solution: toward the plant-mediated biosynthetic mechanism, J. Nanoparticle Res. 13 (10) (2011) 4957–4968.
[49] R. Shukla, S.K. Nune, N. Chanda, K. Katti, S. Mekapothula, R.R. Kulkarni, W.V. Welshons, R. Kannan, K.V. Katti, Soybeans as a phytochemical reservoir for the production and stabilization of biocompatible gold nanoparticles, Small 4 (9) (2008) 1425–1436.
[50] Basset, C. Vadrot, J. Denis, J. Poupon, J. and Zafrani, E. S, Prolonged cholestasis and ductopenia following gold salt therapy. Liver Int., 23: 89–93.
[51] C.F. Shaw, Gold-based therapeutic agents, Chem. Rev. 99 (9) (1999) 2589–2600.
[52] J.F. Hainfeld, D.N. Slatkin, T.M. Focella, H.M. Smilowitz, Gold nanoparticles: a new X-ray contrast agent, Br. J. Radiol. 79 (939) (2006) 248–253.